



Croatian high-resolution monthly gridded dataset of homogenised surface air temperature

Melita Perčec Tadić¹ · Zoran Pasarić² · José A. Guijarro³

Received: 8 March 2022 / Accepted: 7 October 2022 / Published online: 14 November 2022
© The Author(s) 2022

Abstract

Homogenised climatological series and gridded data are the basis for climate monitoring and climate change detection. Considering this, monthly mean temperatures from 122 Croatian stations were homogenised, and high-resolution monthly gridded data were developed for the 1981–2018 period. Homogenisation needs to be performed on stations from the same climate region; therefore, hierarchical clustering is introduced to define those climate regions in Croatia. The breaks of homogeneity were detected by the standard normal homogeneity test on 54 stations. Regression kriging was applied to produce monthly grids for each month in the analysed period. The quality of the interpolation assessed by leave-one-out cross-validation resulted in a root mean square error of 0.7 °C. The quality of spatial interpolation is supplemented with normalised error maps. The derived homogenised station data and monthly grids are necessary for national climate monitoring, the production of climate normals and the estimation of trends. After 1999, average annual anomalies from the 30-year climate standard normal 1981–2010 were positive and up to 1.4 °C warmer than the average and only occasionally negative. The measured amount, sign and significance of the trend were accurately captured on the trend maps calculated from the monthly maps. Significant strong warming was observed and mapped over the entire Croatian territory in April, June, July, August and November. It was stronger inland than on the coast. Annual trends were significant and ranged from 0.3 °C/decade to 0.7 °C/decade. There was no observational evidence of enhanced elevation-dependent warming over elevations from 750 to 1594 m.

1 Introduction

Human influence has warmed the atmosphere, oceans and land, causing rapid and widespread changes in those systems (IPCC 2021). This influence on climate, driven by emissions of greenhouse gases, has been unprecedented in at least the last 2000 years (IPCC 2021). The global surface temperature was 1.09 [0.95 to 1.20] °C higher in 2011–2020 than in 1850–1900, with larger increases over land (1.59 [1.34 to 1.83] °C) than over the ocean (0.88 [0.68 to 1.01] °C) (IPCC 2021).

The focus of this study was to create a homogenised mean monthly air temperature series to produce monthly

temperature grids and to derive climate monitoring products to assess the state of air temperature and the observed temperature change in Croatia. The country is part of the Mediterranean, where the mean temperature is expected to increase at a rate larger than the global mean temperature, particularly in summer (Lionello and Scarascia 2020). Data measured at meteorological stations are representative for describing the climate of the surrounding area of the meteorological station, but only remote sensing methods or spatial interpolation methods (SIMs) can provide estimates where there are no ground observations (Vicente-Serrano et al. 2003; Hofstra et al. 2008). As stated in Haylock et al. (2008), the main reasons for producing gridded data are (1) estimation of the values away from the observation stations, (2) the need for the optimal assessment of the areal averages and (3) validation of the regional climate models (RCMs). Although high-quality gridded climate data are available for monitoring climate and climate change in Europe, either derived from observations such as E-OBS (Haylock et al. 2008) at 6 km resolution or reanalysis such as ERA5 (Hersbach et al. 2020) at 31 km resolution and ERA5-Land (Muñoz-Sabater

✉ Melita Perčec Tadić
melita.percec.tadic@cirus.dhz.hr

¹ Croatian Meteorological and Hydrological Service, Zagreb, Croatia

² Faculty of Science, Department of Geophysics, Zagreb, Croatia

³ State Meteorological Agency (AEMET), Balearic Islands Office, Palma, Spain

et al. 2021) at 9 km spatial resolution, fine-scale analysis using national observed data is often preferred.

In Li and Heap (2014), 38 SIMs applied in environmental sciences are classified as nongeostatistical, geostatistical and combined. Estimation by nearly all SIMs can be regarded as the weighted average of observations (Webster and Oliver 2007). Hijmans et al. (2005) created monthly temperature and precipitation grids using a thin-plate smoothing spline (TPS) algorithm with latitude, longitude and elevation as independent variables. The dataset is expanded with solar radiation, vapour pressure and wind speed in Fick and Hijmans (2017). Multiple linear regression (MLR) was used to produce the temperature climatology of the greater Alpine region, including Croatia, in Hiebl et al. (2009). Longitude, latitude, elevation and distance from the coast were used as the predictors in MLR. The UK monthly gridded dataset of several climatological variables is derived with multiple regression with geographic factors followed by inverse distance weighting of the residual (Perry and Hollis 2005). The Alpine precipitation dataset combined a regression approach for the interpolation of the long-term mean with the interpolation of the daily anomalies by angular distance weighting (ADW) (Frei and Schär 1998). The gridded monthly CRU dataset of several variables also combines long-term grids with monthly anomalies calculated by ADW (New et al. 2000). All these datasets are derived using combined SIMs, which mostly differ in methods for the interpolation of anomalies (IDW, TPS, ADW). Similar is regression kriging (RK) which combines regression on environmental predictors with kriging of the residuals (Hudson and Wackernagel 1994; Knotters et al. 1995; Odeh et al. 1995; Hengl et al. 2003, 2004, 2007; Meusburger et al. 2012; Brinckmann et al. 2016). The RK interpolation method is used for producing the maps of 30-year climate standard normals in the Climate Atlas of Croatia 1961–1990 and 1971–2000 (Zaninović et al. 2008; Perčec Tadić 2010).

In this study, we focus on the mapping of the mean monthly values for a particular month of each year in the period 1981–2018 (38 years). The RK prediction and normalised error maps are calculated for each month. From monthly grids, we calculated climate monitoring products such as climate standard normals for the 1981–2010 period, anomalies from the normal, spatial temperature trends and spatially aggregated anomalies on a country level.

Prior to deriving gridded data that can be used for climate monitoring and trend estimation, station data need to be checked for inhomogeneities and homogenised if needed. Homogenisation based on long meteorological time series is often regarded as the first stage in climate monitoring and climate variability and change detection (Alexandersson and Moberg 1997). Inhomogeneities in the data series can be regarded as anomalous perturbations not related to climate variability. One type of inhomogeneity is a sudden shift in

the mean compared with surrounding sites. Such shifts are often related to relocations of the station, changes in the local environment, observation practices or data processing but can also be the result of digitization and database errors (WMO 2020). Reviews on the different methodologies for dealing with inhomogeneities consider the standard normal homogeneity test (SNHT) widely used and among the better performing inhomogeneity detecting methods (Peterson et al. 1998; WMO 2003; Beaulieu et al. 2008).

SNHT was used in Likso (2003), who examined homogeneity of the annual temperature series from the 1949–1998 period on ten Croatian stations revealing the breaks in all but one station (Zagreb-Maksimir). Pandžić and Likso (2010) analysed the abrupt and gradual linear change in annual mean temperatures from the 1961–2000 period at 22 Croatian stations using the modified SNHT, where breaks were detected at all but five stations. Our preliminary research (Nimac and Perčec Tadić 2017) revealed breaks in homogeneity on half of the 39 air temperature time series from the 1981–2010 period. The change in long-term seasonal and annual temperature means among homogenised and nonhomogenised series was statistically significant at only one station (Nimac and Perčec Tadić 2017). However, the changes in trend revealed that homogenisation changed the amount but also the statistical significance of the trend. Positive trends become significant, while negative ones become not significant after homogenisation. Coefficients of correlation among pairs of stations became higher and more similar due to homogenisation. In this study, the robustness of the homogenisation method was tested, while the dataset was extended to 122 stations and to a longer time period.

The study was organised as follows: in Sect. 2, we describe the main characteristics of the country and the data. In Sect. 3, we describe the clustering, homogenisation and spatial interpolation methods, the accuracy measures and the climate monitoring products to be derived. Sect. 4 presents the results of the applied methods. In Sect. 5, we present selected national climate monitoring products. The discussion and conclusions are presented in Sect. 6. The table with station metadata and a list of breaks is presented in Appendix. The charts of the time series of the original and homogenised data are provided in Online Resource 1.

2 Data

Croatia is a southeastern European country situated on the eastern coast of the Adriatic Sea with a Dinaric ridge separating its maritime from the continental part, which belongs to the Pannonian Basin (Fig. 1). This defines several climatic factors that shape the climate of Croatia:

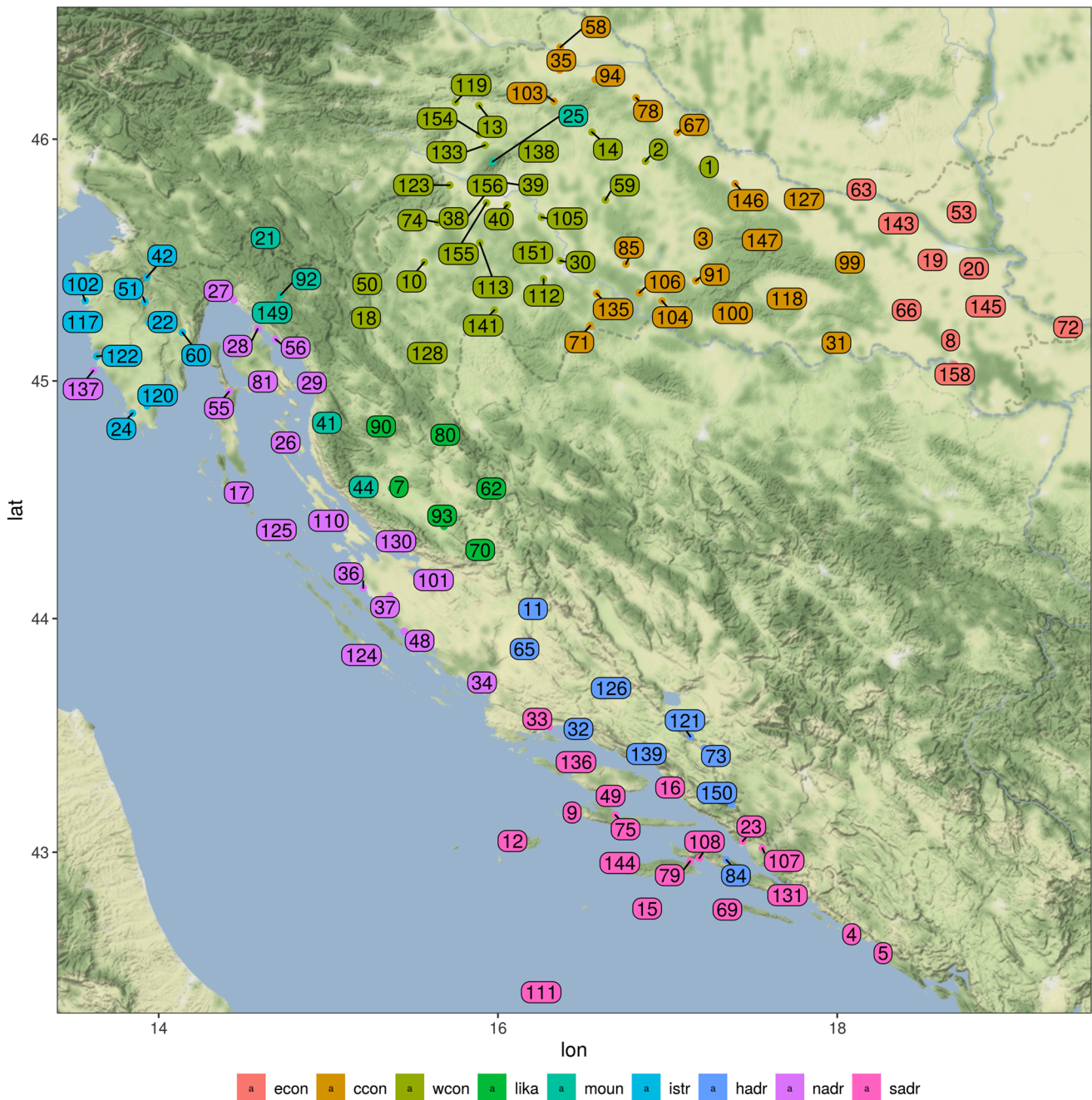


Fig. 1 Map of Croatia and meteorological stations divided into nine regions based on the clustering algorithm: eastern continental (*econ*), central continental (*ccon*), western continental (*wcon*), Lika plateau (*lika*), mountainous (*moun*), Istria (*istr*), Adriatic hinterland (*hadr*),

northern Adriatic (*nadr*) and southern Adriatic (*sadr*). The colour of the symbols denotes a region, while the number inside the symbol is the ID of the station

diverse orography ranging from 0 to 1700 m, position at the coast of the Adriatic Sea, longitude and latitude (Figs. 2 and 3 in Perčec Tadić 2010). The result was a large mean annual temperature span over a small country, from 4 °C in the mountains to more than 17 °C along the coast for the normal period of 1981–2010. These spatial temperature differences with the cold elevated locations,

slightly warmer continental areas and even warmer Adriatic coast with the warmest southern Adriatic are to be modelled for the entire territory with the proposed spatial interpolation method. Standard deviations of the mean annual temperature are up to 0.8 °C, compared to 0.4 °C at the coast, where variability is lower due to maritime influence.

Data used in this study were monthly mean temperatures from 122 Croatian main and climatological meteorological stations from the period 1981–2018 (station positions are denoted by circles in Fig. 1). There were 27% of stations with complete data records, but the stations with missing data were also used if at least 25 years of data are available. Croatian land fits in a square of approximately $466 \times 462 \text{ km}^2$, but due to its peculiar shape, its area is just $57\,750 \text{ km}^2$. If the distribution of the stations would be regular in space, there would be one station on each $22 \times 22 \text{ km}^2$. However, the density of the meteorological stations was uneven across the country and not perfectly balanced across the elevation range (Figs. 4 and 5 in Perčec Tadić 2010).

3 Methods

The present study addresses (1) the homogenisation of monthly temperature data measured at the stations, (2) spatial interpolation to a regular 1 km grid and (3) calculation of the gridded climate monitoring products. The R framework (R Core Team 2020) was used for calculations and visualisations. The main packages used were *climatol* (Guijarro 2019) for homogenisation, *gstat* (Pebesma 2004; Gräler et al. 2016) and *automap* (Hiemstra et al. 2009) for spatial interpolation, *raster* (Hijmans 2020) for raster manipulations and calculations and *spatialEco* (Evans 2020) for spatial trend analysis.

3.1 Clustering

For the homogenisation method to be reliable, homogenisation must be performed on data with similar climate regimes (Mamara et al. 2013; Marcolini et al. 2019; Guijarro 2021). Ward's hierarchical clustering or the method of minimum variance (Ward 1963) was performed to group stations according to the similarity in temperature regimes, which was shown to be a first approximation of the climate regions. We were looking for clusters of stations that have similar sequences of temperature differences for consecutive months. Similarity between sequences was measured by ordinary Euclidean distance. The method started from a single sequence in each cluster and iteratively merges sequences based on minimal distance. Ward's algorithm assures that intragroup similarity is maximised while intergroup similarity is minimised. The clustering results with a selected number of clusters that are expected to contain stations with the most similar temperature series and hence are suitable for further homogenisation inside the clusters.

3.2 Homogenisation

Homogenisation can be performed by comparing each candidate series with another station series or with a composite reference series. Among several methods used in the large MULTITEST project, the ACMANT method provided the most accurate homogenisation of individual time series, resulting in the reconstruction of local climate variability (Domonkos et al. 2021; Domonkos 2021). This method was closely followed by *climatol*. Both methods use composite reference series, while pairwise methods using a single reference series seem to be more efficient for the detection of the mean climatic trends over large geographical regions (Coll et al. 2020; Domonkos et al. 2021; Domonkos 2021). Among the homogeneity tests, the SNHT has been used quite extensively (Venema et al. 2012; Mamara et al. 2013; Kolendowicz et al. 2019; WMO 2020; Coll et al. 2020). In the R package *climatol* used in this paper, the SNHT was applied to the differences between candidate and composite reference series, both in the normalised form, to reconstruct local climate variability (Guijarro 2019, 2021). The normalisation was calculated by subtracting the mean and dividing it by the standard deviation over the entire data series of 456 months (38 years). In the first homogenisation stage, the SNHT was applied iteratively on overlapping windows of 120 terms sliding forward by 60 terms, which is one way of detecting multiple breakpoints in one series. In the second stage, the test was applied to the whole series. In the process, the series were split into two fragments at the position where the test values were above the SNHT threshold. Thresholds for the SNHT statistic T were denoted by SNHT1 for the first stage and SNHT2 for the second stage (Guijarro 2019). For our sample size, the listed critical values of the SNHT statistic T for a 95% confidence level would be 9.33 for a first stage over 120 terms and 10.272 for a second stage over 450 terms (closest to our samples' size of 456 months), according to Khaliq and Ouarda (2007). These are theoretical thresholds simulated from large sets of random normal numbers with up to 50,000 members by Khaliq and Ouarda (2007), similar to Alexandersson and Moberg's (1997) thresholds for series up to 200 members. However, the range of the estimated SNHT T values in our real-world dataset was much larger, presumably due to deviation from the theoretical randomness (Mamara et al. 2013), with values comparable to those suggested in Meseguer-Ruiz et al. (2018) and Curci et al. (2021). Consequently, we chose to test several critical T values that were higher than theoretical, where higher values correspond to less strict break detection criteria. There were several options for selecting the final homogenised series, and we selected the series with the original data being retained at the end of the series, as in Marcolini et al. (2019) and Meseguer-Ruiz et al. (2018).

3.3 Regression kriging

Regression kriging (RK) is a combined SIM (Li and Heap 2014) that accounts for large-scale spatial variability through the dependence of the target variable on the spatial predictors. Additionally, it accounts for the local, or small-scale, part of the remaining variability through the model of spatial autocorrelation. The procedure can be described in four steps: (1) assess the relationship of the dependent variable (monthly temperature) with climatic factors of altitude, distance to the sea, latitude and longitude (predictors) through multiple linear regression (MLR), (2) establish the variogram model of spatial autocorrelation of residuals ($\hat{\epsilon}$) where residuals are the differences between observed values and the values predicted by MLR, (3) evaluate the accuracy of predictions with leave-one-out cross-validation on station locations, and (4) calculate prediction maps and normalised error maps (Hengl et al. 2004; Perčec Tadić 2010). In the process, only the significant predictors in the MLR model were retained based on a t test applied to the regression coefficients under a significance level of 0.05. The remaining residuals were interpolated by kriging.

The sample variogram was calculated from residuals for regular distance intervals (bins) $[h_j, h_j + \delta]$ by the semivariance:

$$\hat{\gamma}(\bar{h}_j) = \frac{1}{2N_j} \sum_{i=1}^{N_j} (\hat{\epsilon}(s_i) - \hat{\epsilon}(s_i + h))^2, \forall (s_i, s_i + h) : h \in [h_j, h_j + \delta]. \quad (1)$$

Here, the spatial locations of stations were denoted by s_i , where N_j is the number of station pairs separated by a distance h belonging to interval $[h_j, h_j + \delta]$, and \bar{h}_j is the average of all N_j h 's (Pebesma 2014).

Four variogram models were tested by default while fitting the variogram model to the sample variogram: spherical, exponential, Gaussian and Matern. The initial variogram parameters, *nugget*, *partial sill* and *range*, were estimated from the data automatically. The fitting of the variogram model was controlled by adjusting the minimum number of points in a bin, *min.np.bin* (Hiemstra et al. 2009). The default value of five points was too low for our spatial data configuration. In many months, the first to the third bin in the sample variogram would produce too jittery semivariance, so the optimal value was selected as one that minimises the RMSE of the mean temperature through leave-one-out cross-validation (*loocv*). For interpolation of the residuals that remain after MLR, we adopted an option of kriging in a local neighbourhood, while point kriging and kriging of the block mean values are also available (Pebesma 2004; Hiemstra et al. 2009; Gräler et al. 2016). The default setting of using all observations for the prediction at each grid cell is not optimal for a peculiarly

shaped and climatologically diverse country such as Croatia; hence, we carefully balance the number of the nearest observations, *nmax*, and the maximum distance from the prediction location to the observations, *maxdist*, to avoid the stations from a climatologically different region. The optimal values were selected through *loocv* as for the optimal *min.np.bin*.

3.4 Accuracy assessment

The performance of the multiple linear regression model is evaluated through the coefficient of determination R^2 adjusted for the number of predictors (Draper and Smith 1998). The RK performance at the prediction locations was again assessed through the *loocv* procedure. The mean error (ME) and root-mean-square error (RMSE) were calculated at prediction locations:

$$ME = \frac{1}{l} \sum_{j=1}^l [z(s_j) - \hat{z}(s_j)] \quad (2)$$

$$RMSE = \sqrt{\frac{1}{l} \sum_{j=1}^l [z(s_j) - \hat{z}(s_j)]^2} \quad (3)$$

where the observed temperatures at spatial locations s_j were denoted by $z(s_j)$ and the *loocv* predictions by $\hat{z}(s_j)$, while their differences were called residuals. The standard deviation of the observations is denoted by σ_z . Comparison of the RMSE across the months is performed through RMSE normalised by the standard deviation of observations:

$$RMSEr = \frac{RMSE}{\sigma_z}. \quad (4)$$

As a rule of thumb, we consider that prediction is accurate if $RMSEr < 0.4$ (Hengl et al. 2004), in which case the accuracy defined by

$$accuracy = 1 - RMSEr^2 \quad (5)$$

is above 84%. The normalised kriging error map is calculated as the square root of the prediction variance map divided by the standard deviation of the prediction variable (Burrough et al. 1998; Hengl 2009; Perčec Tadić 2010). A normalised prediction error lower than 0.4 is considered a satisfactory prediction since in this case, the model predicts more than 84% of the total variation. Otherwise, if this error was above 0.8, the model accounts for less than 36% of the variation (Hengl 2009). Those errors also propagate and affect the derived climate monitoring products. On the stations' locations, the effect of the errors can be noticed as differences between measured and interpolated values.

3.5 Climate monitoring products

Climate standard normals (monthly means) and trends are calculated from the homogenised station data. Gridded climate standard normals were calculated from the monthly grids as a mean over the period 1981–2010, from which the grids of monthly anomalies are calculated by subtracting the monthly climate standard normal grid from each monthly grid. The derived spatial means of monthly anomalies aggregated over the country were among the most important national climate monitoring products (WMO 2017a).

Temperature trends and their significance were calculated from the monthly grids over the period 1981–2018. Theil-Sen slope was calculated to estimate the trend over 10 years, and the Mann-Kendal test was used to assess its significance (under the significance level 0.05). The nonparametric Pettitt rank test (Verstraeten et al. 2006) was applied to temperature anomalies to estimate a year when a change in the mean temperature appears over Croatia. The areas on the maps where the trends were not significant were displayed using 50% transparency. The normals and trends calculated from the homogenised station series were presented on the corresponding gridded maps.

4 Results

4.1 Clustering

Hierarchical clustering was performed to group the stations according to similarity in temperature regimes, which was a prerequisite for further homogenisation. Starting from the smallest possible number of clusters, i.e., two, we can distinguish the maritime and continental temperature regimes (not shown). Going down the dendrogram tree, more details about the climate characteristics appear. With three clusters, the continental cluster was divided between continental lowland and the mountainous region, leaving the maritime cluster unaffected. With four clusters, differences between the northern and southern Adriatic data regimes appear in maritime clusters. With five clusters, we can see that most of the eastern part of the continental lowland (*econ*) was different from the rest of the central and western continental regimes. With six clusters, the southern Adriatic cluster was split into the hinterland (*hadr*) and coast (*sadr*). With seven clusters, the mountain region was split into the Lika Plateau (*lika*) and higher mountain tops (*moun*). Eight clusters revealed that the Istria Peninsula (*istr*) was distinct from the rest of the northern Adriatic stations (*nadr*), and finally, nine clusters reveal a small distinction between the western (*wcon*) and central-northern continental (*ccon*) lowland (Fig. 1). Even though the temperature series of the last two clusters were similar, we decided to separate them to have a more balanced

number of stations across the clusters. We did not proceed with a larger number of clusters since for ten clusters, some microlocation characteristics emerged on southern Adriatic islands that were too local to be investigated in this research. After the nine regions with similar temperature regimes were determined, homogenisation was performed for each region separately. We note that the stations in each cluster were also grouped geographically, although geographical locations were not explicitly included in the algorithm. A notable exception was the region *moun* covering the mountain tops, which also includes station Puntijarka (ID = 25, h = 988), which geographically belongs to the *wcon* region but is nevertheless characterised as a mountain station. This showed that the clusters were also well aligned with the orography. Consequently, the obtained clusters can be recognised as a first approximation of the climate regions.

Coefficients of correlation over the pairs of nearest stations in the same region are above 0.9, supporting the similarity inside the clusters and gradually decrease with the distance between the stations.

4.2 Homogenisation

Due to the limitations of the SNHT thresholds derived from synthetic series, we tested the robustness of the test by choosing six combinations (denoted as *test1* to *test6* in Table 1) of the SNHT thresholds for the two stages of homogenisation. It appeared that this affects the number of detected breaks of homogeneity. *Test1* with the highest SNHT threshold allowed for more variation between the candidate and the reference series and hence the smallest number of breaks. In that case, 70 breaks were detected in all regions. *Test6*, with the lowest SNHT threshold, was the strictest in break detection, with 288 breaks suggested over the regions. Setting the SNHT threshold as in *test6* would result in a higher level of homogeneity and smoother spatial temperature fields.

Without quality metadata, there is no objective decision on which SNHT threshold combination to choose. However, homogenisation makes the temperature trends more uniform across the region (Nimac and Perčec Tadić 2017), so we compared the trends for datasets where only missing data have been interpolated (OR stands for original in Fig. 2) with trends for *test1* to *test6*, which are expected to be changed by homogenisation. We showed the comparison for *test1* (HO stands for homogenised in Fig. 2), which already reduced the largest isolated negative trends in dataset *test0* (OR in Fig. 2) in September and October, including one in September that was marked as significant (Station 141). Most positive isolated significant trends in *econ* and *ccon* in May were reduced to nonsignificant ones. The same happened in *wcon* in March and in *lika*, *istr*, *hadr* and *sadr* in January. Reduced were also isolated positive significant

Table 1 Comparison of the number of detected homogeneity breaks depending on the SNHT statistic T for the nine regions (columns from *econ* to *sadr*) and the total sum of breaks over all nine regions (sum) for the six tests performed. In the SNHT column, the first number is SNHT1, and the second is SNHT2

test	SNHT	econ	ccon	wcon	lika	moun	istr	hadr	nadr	sadr	sum
test1	(35, 70)	3	14	21	3	1	5	6	9	8	70
test2	(35, 35)	11	18	26	4	4	7	10	12	17	109
test3	(25, 50)	12	24	34	7	1	10	8	13	18	127
test4	(25, 25)	18	28	44	8	5	14	13	16	24	170
test5	(15, 30)	22	46	60	9	7	19	17	26	29	235
test6	(15, 15)	24	55	75	13	9	20	24	32	36	288

trends in *hadr* in February and in *hadr* and *sadr* in October. Nevertheless, several negative trends, although not significant at the 0.05 level, remain during September, October and December. However, those were the months with the smallest positive and sometimes negative temperature trends compared to other months in the entire Croatian territory. Using more strict SNHT thresholds (*test2* to *test6*) makes trends' significance more spatially homogenous in some but not in all regions, so *test1* SNHT thresholds are used further in the analysis for break detection and homogenisation.

The inventory of detected breaks for all the stations is presented in Appendix together with the percentages of the original data, missing data that were interpolated and the data created during homogenisation. The breaks were detected in 54 out of 122 data series. Altogether, 70 breaks were identified. There were 41 stations with one identified break, 10 stations with two breaks and three stations with three identified breaks.

It was preferable that stations with many breaks and/or with a substantial percentage of altered original data were not clustered in space. Indeed, Fig. 3 shows a balanced spatial distribution of high-quality stations with no breaks (circles) and a small percentage of interpolated missing data (blue symbols). The less favourable situation can be noticed in *ccon*, *wcon*, *sadr* and *hadr* regions where there are clusters of stations with more than 40% of altered data (yellow, orange or red symbols in Fig. 3).

A comparison of the monthly percentage of the original, homogenised or interpolated (missing) data is presented in Fig. 4. The percentage of missing data in each month shows that from 1981 to July 1991, approximately 10–15% of the overall monthly data from the 122 stations were missing. These data were interpolated. In 1991, the war in Croatia started, and then the largest drop in the percentage of available data occurred, with 30% of stations missing in September 1991 and 35% missing in December 1991 and January 1992. Around July 1994, the percentage of missing data was approximately 20%, dropping to 10% in 1997 and to 5% around October 2000. Until 2015, this was the observation period with the most data available. After that, the

percentage of missing data slightly increased due to four stations that were closed in 2014 and 2015.

The decision to keep, for climate monitoring purposes, the homogenised series that have the original data at the end of the period was reflected in the monthly share of the data altered by the homogenisation. The percentage of data was larger at the beginning of the period, from 1981 until July 1991, when approximately 30–40% of stations were homogenised in a month. Until 2000, approximately 20–30% of the monthly data were homogenised, dropping to 10–20% from 2000 until 2006. After that, the percentage of the homogenised data was below 10% in a month (Fig. 4).

A detailed comparison of the original and homogenised series for each station is provided in Online Resource 1. Those charts were also used to visually check if there are some large alterations of the data after homogenisation. Without available digitized metadata of dates of relocation, change of the observer or change in the environment to assist break detection, it is advisable to try to confirm at least the largest proposed changes by consulting published breaks or the available paper metadata reports, which is discussed in Sect. 6.

The differences between the original and homogenised series were used to calculate the ME and RMSE at the station and regional levels to assess the effects of homogenisation. The substantial portion of the data without any adjustment is disregarded from ME and RMSE calculations since they would mask the overall size of the adjustments. The ME calculated from differences of HO and OR data (adjustment) was mostly negative with a median of -0.5–0.0 °C (lower HO than OR, mostly in the beginning of the period) except for *econ* and *lika* regions where a median of ME was 0.3 °C and *istr* with 0.4 °C (Fig. 5a). Median RMSEs were 0.2–0.5 °C except for *hadr* with 0.72 °C (Fig. 5b).

4.3 Regression kriging

Due to the differences in temperature regimes across climatological regions, we preferred to develop kriging in a local neighbourhood. Therefore, we needed to select the optimum maximum distance (*maxdist*) and the number of

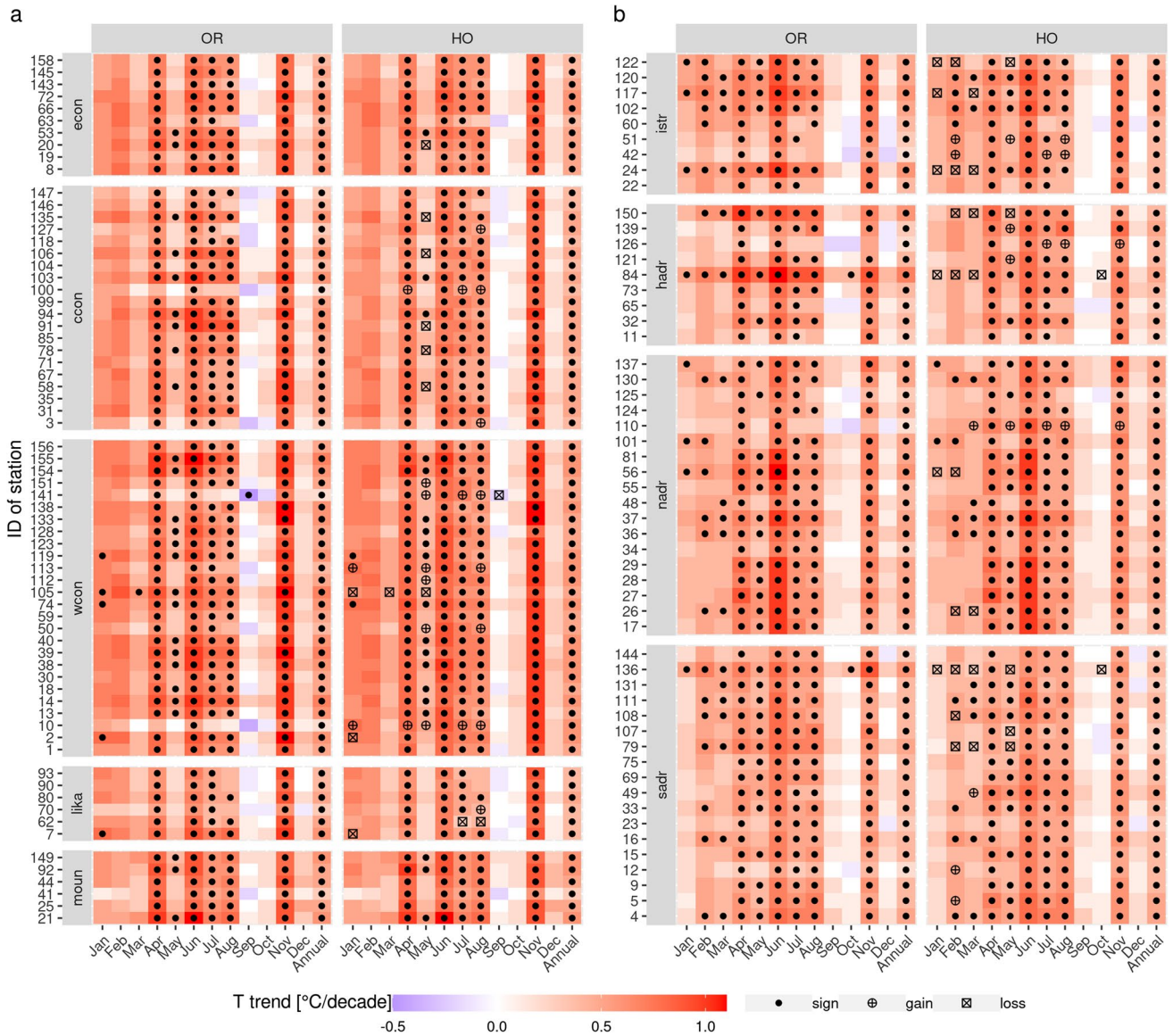


Fig. 2 Trends (colour) and significance at the 0.05 level (symbols) in mean monthly and annual temperatures for the stations in continental and mountainous (a) and coastal (b) regions. On the OR (original data) panels, the point symbol denotes whether the trend in the original data is significant. On the HO (homogenised) panels, the symbols

also denote the change of the significance of the trends between OR and HO datasets: symbol *sign* denotes the significant trend in both datasets, *gain* shows that trend changed from nonsignificant to significant and *loss* if the opposite happened. For nonsignificant trends, no symbol is used

nearest neighbours (*nmax*) to be used for kriging in each grid cell. Additionally, for the variogram estimation, the minimum number of point pairs over the bins of the distances was optimised (*min.np.bin*). Possible values need to consider the approximate size of the region that is a square of 400 × 400 km, the peculiar shape of the country, the number of stations available in each grid point (Fig. 6) and the assumption that based on climatic differences, we prefer not to use stations from the coast to predict temperature in continental Croatia and vice versa (Zaninović et al. 2008).

We determined the number of neighbouring stations for various search radii between 20 and 400 km with a 20 km step. For the example of a search radius of 100 km, there are more than 40 stations available for local interpolation in the western continental region but not more than 10 over peripheral parts of the domain (Fig. 6). This was to be considered when optimising the parameters for kriging in a local neighbourhood.

Optimisation of the RK parameters was conducted for a minimum number of points in a bin for variogram estimation

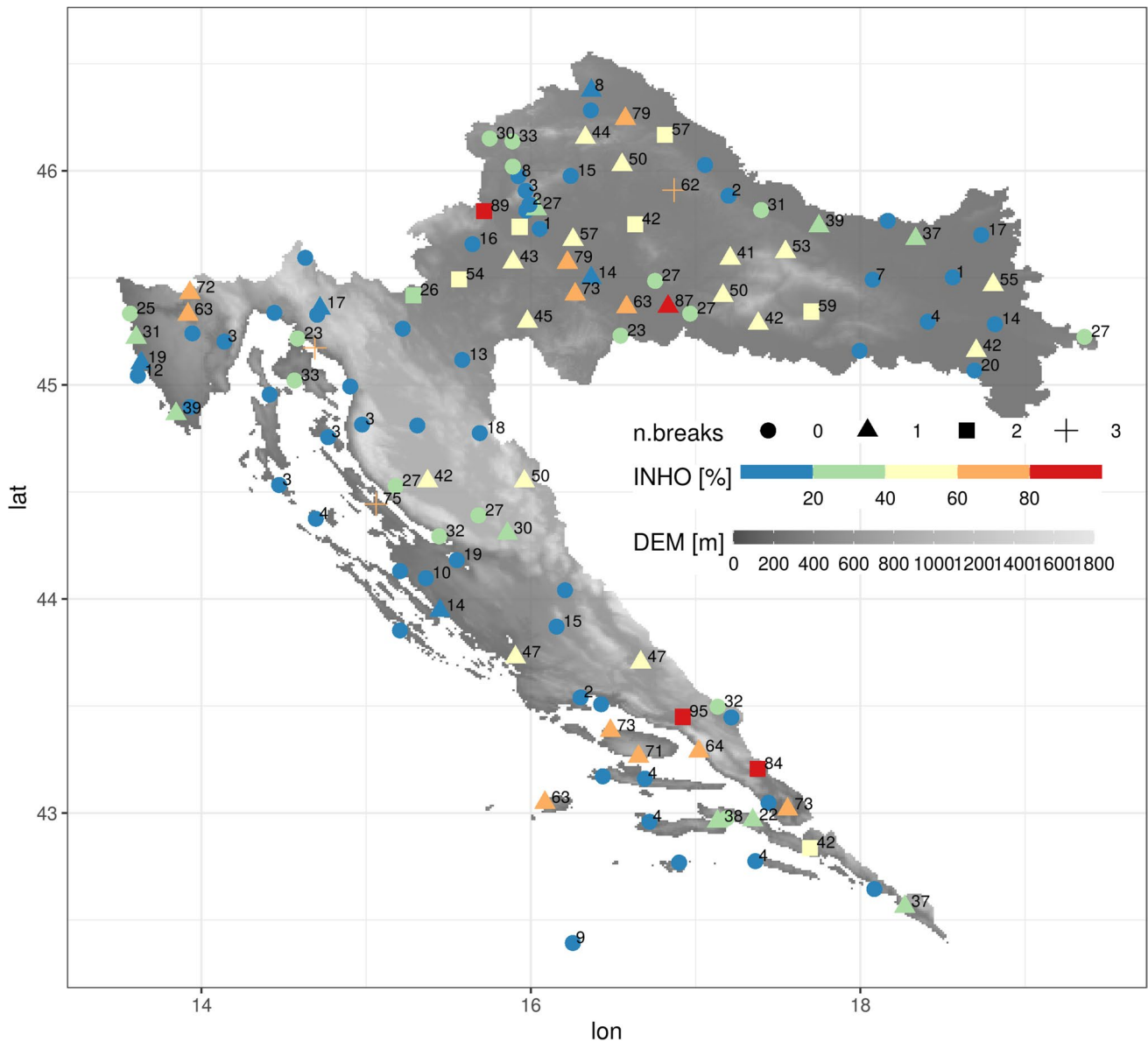


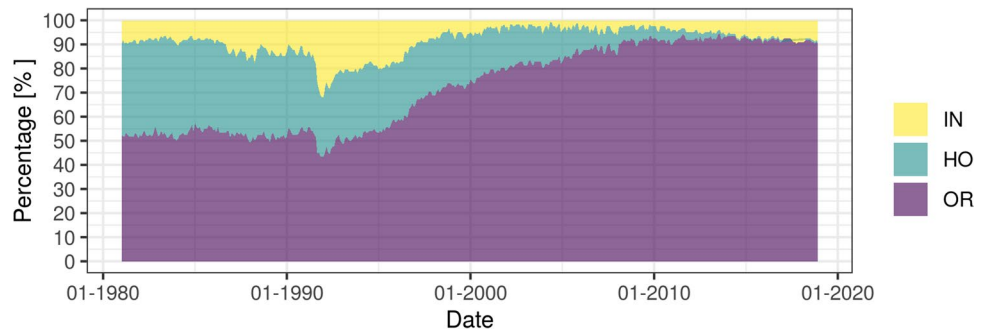
Fig. 3 Spatial distribution of stations according to the number of breaks (*n.breaks* denoted by symbols' shape) and according to the percentage of interpolated and/or homogenised data (*INHO*, denoted

by symbols' colour and label text). The map in the background shows the orography (*DEM*)

(*min.np.bin*) and for the maximum number of points (*nmax*) and maximum distances to the points (*maxdist*) to be used for kriging predictions. The parameters tested were $min.np.bin \in \{40, 50, 60\}$, $maxdist \in \{80, 120, 160, \dots, 400\} \times 1000m$ and $nmax \in \{5, 15, 20, \dots, 120, 122\}$, giving a total of 351 combinations for each month. The performance was evaluated with *loocv* RMSE, and all tree *min.np.bin* values were shown to be equally good (not shown). When setting $nmax=5$ or $maxdist=80 km$, the RMSEs were above 10 °C, so those were excluded from further consideration. The RMSEs averaged over the locations and *min.np.bin* for each of the remaining combinations of *nmax* and *maxdist* were lower than 0.9 °C

(Fig. 7a and b). The selection of the optimal *maxdist*, among those longer than 120 km, is no longer as sensitive (Fig. 7a). The optimal *nmax* was found to be 45 or 55 (Fig. 7a and b). Setting it higher than 55 will not affect RMSE too much, while setting it lower than 45 will increase RMSE by approximately 0.2 °C. Finally, 34 out of 351 combinations were selected as the best combinations for all 456 months based on the lowest RMSE. The combination of the parameters $min.np.bin=40$, $nmax=45$ and $maxdist=160 km$ (40_045_160) was selected as the best in 28.9% months, followed by 40_055_160, which was the best in 18.9% of months. The RMSEs were slightly higher in winter months and in November.

Fig. 4 The monthly percentage of original (OR), homogenised (HO) and interpolated (IN) data



This decrease in the final number of optimal combinations to 34 suggests a possible simplification. Namely, one can choose the best combination of the parameters for each calendar month (12 models) or even a single combination for all months in the dataset. The impact of these simplifications on the *loocv* RMSE is shown in Fig. 8. Overall, the medians of RMSEs were the lowest from March to July (0.5–0.6 °C), reaching 0.8 °C in Jan and Dec, with bulk values below 0.9 °C (Fig. 8). It is seen that the simplification increased the RMSE by less than 0.05 °C. Based on this, we selected a single set of parameters (40_045_160) to be used for kriging in a local neighbourhood for all months.

The next step was to select the variogram model. The optimal variogram model for each month is selected among four models and fitted to an experimental variogram. Matern (Ste) is the best model for 63% of the months, followed by Spherical (Sph) in 26% of the months and Gaussian (Gau) in 10% of the months, while the Exponential (Exp) model is selected as the best one only once. The *nugget* values were 0.0–1.5 °C, the *partial sill* was 0.0–1.1 °C, and the variogram *range* was 10–300 km. The *nugget* was larger than 1.5 °C for cases of 12/1998, 11/2011, 12/2015 and 12/2016, the *partial sill* was larger than 2 °C for 4/1995, and there were two infinite *ranges* for 4/1995 and 3/2000. They were used as such for the gridding since they did not blow up the *loocv* RMSE.

The median of the monthly adjusted R^2 is above 0.9 in all months, suggesting that the high proportion of the spatial variability is explained by the climatic factors through MLR (Fig. 9a). The accuracy of RK (Eq. 4 and 5) based on the *loocv* RMSE was above 0.84 throughout the year (Fig. 9b) and was slightly higher in the cold part of the year. Recalling Eq. 5 and that the accuracy is higher if the RMSE was lower, we would expect a higher accuracy in the warm part of the year (recall Fig. 8). However, since the accuracy was calculated from RMSE normalised by the variance of the data (Eq. 5), a higher variance of the data reduces the RMSE (Eq. 4) and increased the accuracy, leading to higher accuracy during colder months (Fig. 9b).

Final regression kriging prediction and normalised error maps were presented for the two selected months, a winter month and a summer month, which had the largest warm anomalies in the whole dataset (Fig. 10). The regression kriging predictions (maps in Fig. 10a and c) were in line with the observations (circles in Fig. 10a and c). Somewhat higher normalised errors (Fig. 10b and d) were found over

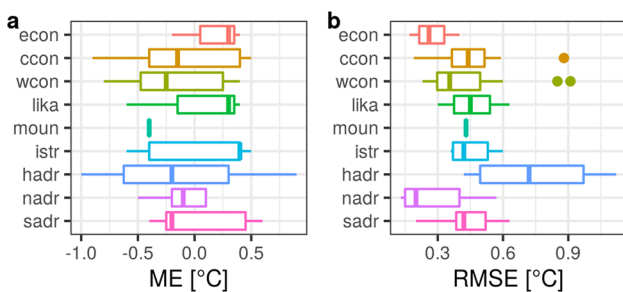


Fig. 5 The mean error (a) and root mean square error (b) calculated from differences in measured and homogenised data for the regions. Only values that are changed by homogenisation are used in the calculation of ME and RMSE

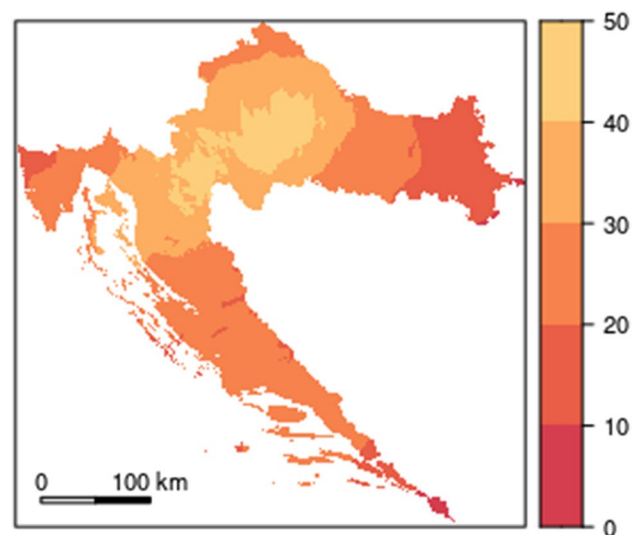
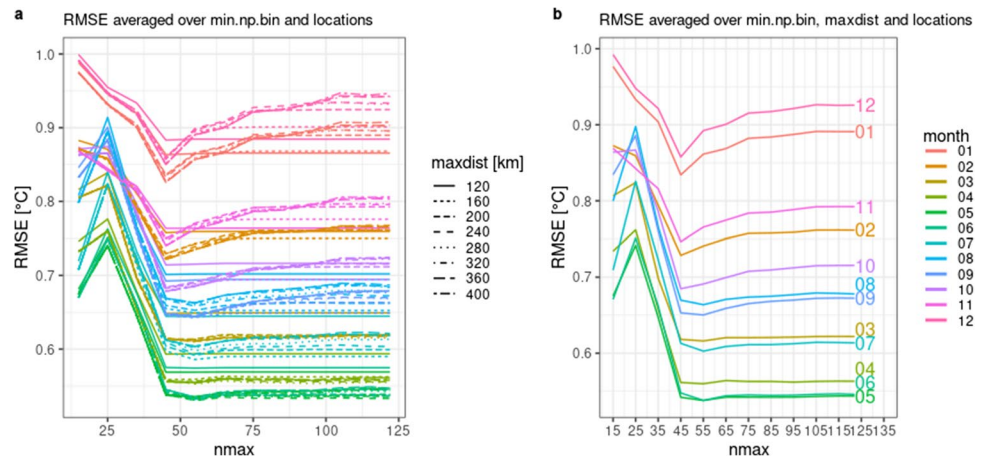


Fig. 6 The number of neighbouring stations available for interpolation in each grid cell for a search radius of 100 km

Fig. 7 *Loocv* RMSE for the optimisation of the RK parameters. Change in monthly RMSE over *nmax* for different *maxdist* (a). Change in monthly RMSE averaged over *maxdist* (b). Colour coding is the same for figures a and b and refers to months



isolated mountains in eastern continental Croatia and over the Adriatic coast. We suspected that prediction accuracy can be improved only by additional measurements.

5 Climate monitoring products

In this section, we present and discuss several climate monitoring products that can be operationally derived from homogenised station data as well from a series of monthly

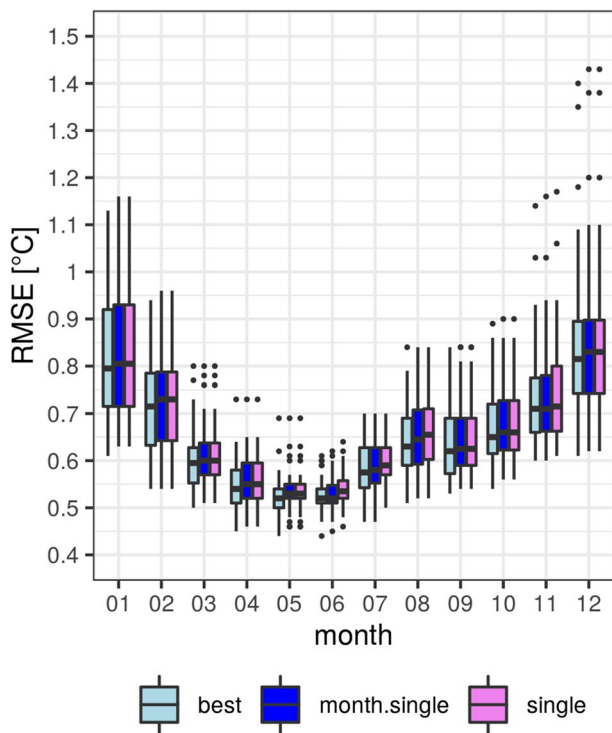


Fig. 8 Comparison of the monthly *loocv* RMSE for three sets of experiments: the best RK parameter combination for each month (best), a single combination for each calendar month (month.single) and a single combination for all months (single)

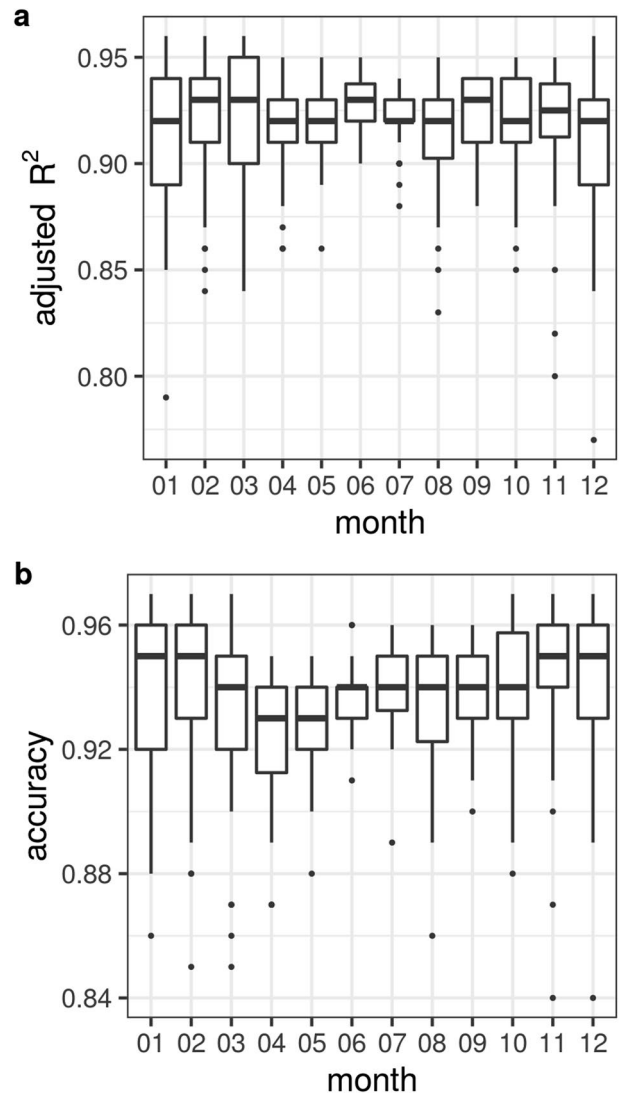


Fig. 9 Adjusted R^2 of the MLR Model (a) and *loocv* accuracy for RK (b)

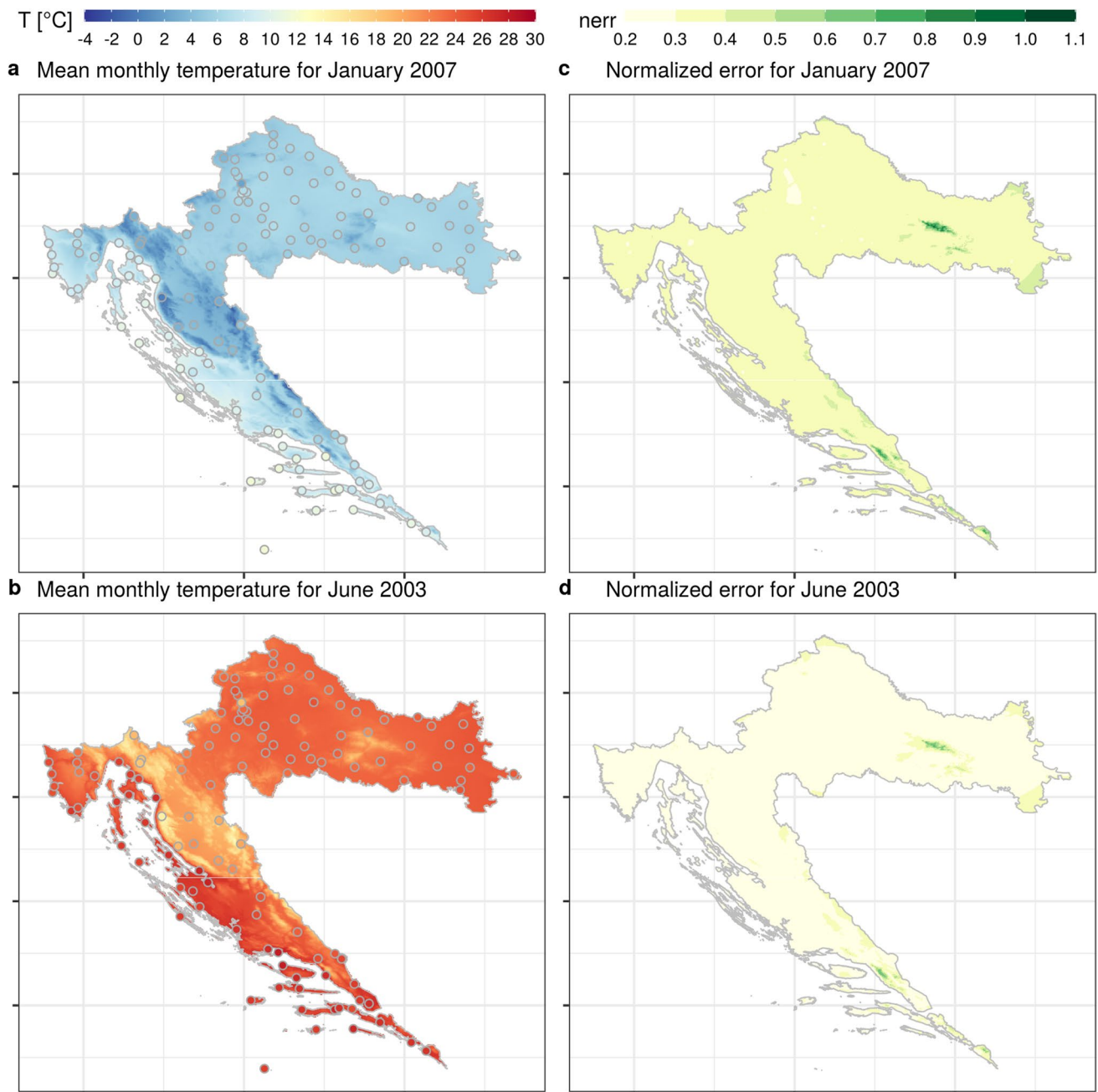


Fig. 10 Prediction (a, b) and normalised errors (c, d) for the months with the most pronounced warm temperature anomalies in winter (January 2007, a and c) and summer (June 2003, b and d)

maps. Some of the most important national climate monitoring products are the *monthly and annual climate standard normals* (WMO 2017b). Here, we highlighted the main seasonal and regional temperature characteristics deduced from the homogenised stations' normals for the 1981–2010 period (Fig. 11).

Winter: In continental Croatia (*econ*, *ccon* and *wcon*), the coldest winter month is January (Fig. 11). Then, follow slightly less cold December and February. In *lika* and *hadr*,

January was the coldest, while December and February temperatures were almost the same. Over the *moun* region, January and February are equally cold. The exception was the highest mountain station (Zavižan, ID=41), where the coldest is February, followed by January and December. Near and on the coast, in *istr*, *nadr* and *sadr*, the coldest months are January, February and December in that order, with January and February temperatures being almost the same at many stations.

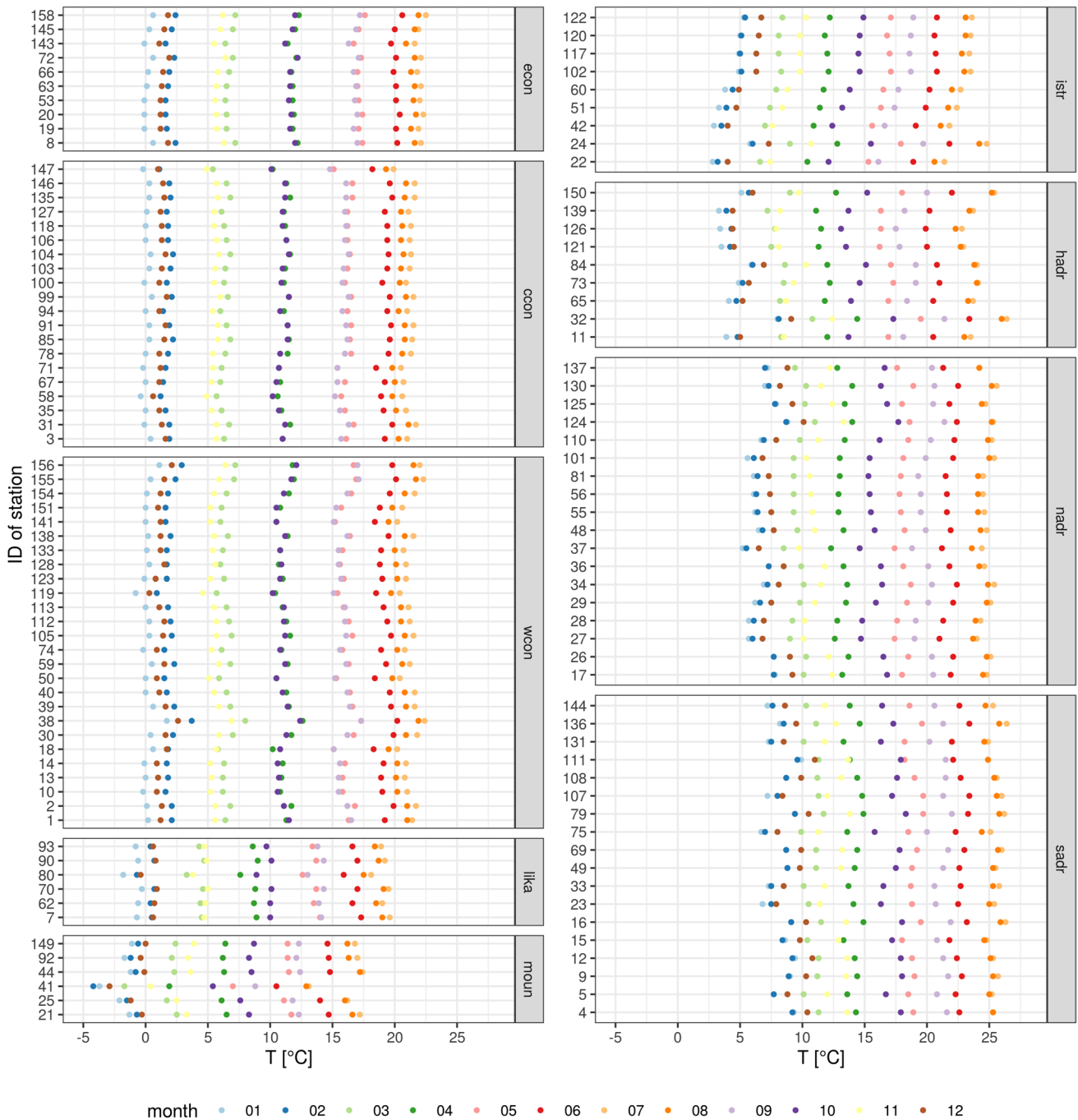


Fig. 11 Annual course of homogenised monthly temperature data. Stations are grouped according to regions. Continental and mountainous regions are on the left, and maritime regions are on the right. Months are differentiated by the colour of the symbols

Spring and autumn: The spring/autumn pairs of months: Mar/Nov, Apr/Oct, May/Sep have very similar temperatures in continental Croatia, with spring months being slightly warmer than their autumn pairs primarily due to longer days. The exception was Ogulin (ID=18, alt=328 m), with monthly temperatures closer to the continental regime but with warmer autumn than spring months, which are the characteristics of the intermittent *lika* and *moun* region. This is

the result of its position on the border of those regions. In intermittent *lika* and *moun* regions, the differences between spring/autumn months are larger compared to continental regions and in favour of warmer autumn pairs (showing already present maritime influence). In maritime Croatia (*istr*, *hadr*, *nadr*, *sadr*), the autumn is even warmer than spring, compared to *lika* and *moun* regions. In spring, the land is getting warmer, but the colder sea is slowing down the

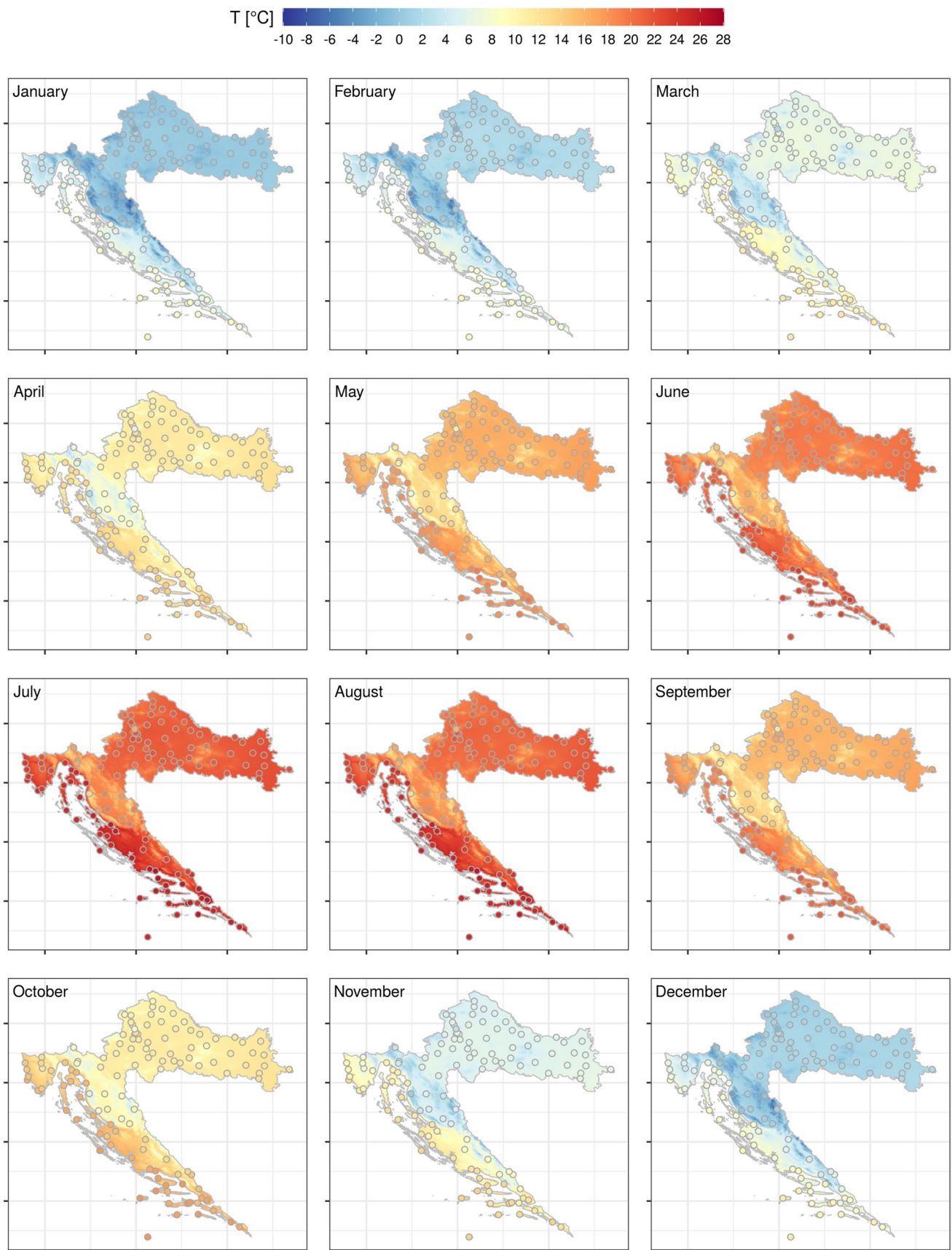


Fig. 12 Maps of mean monthly temperatures for the period 1981–2010. Each map also shows homogenised station normals

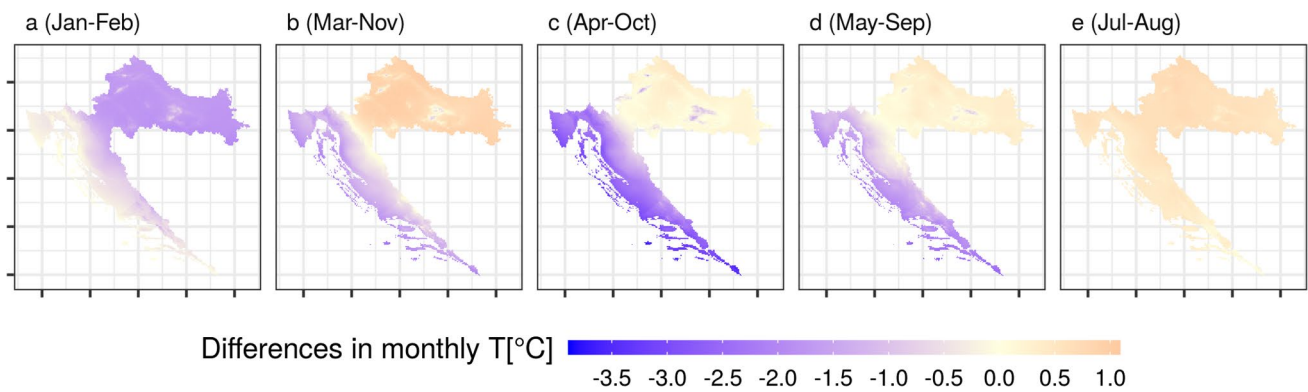


Fig. 13 Differences between mean monthly temperatures for the period 1981–2010. Shown are differences between the two coldest months, Jan-Feb (a), and then differences for the pairs of spring and

autumn months with similar temperatures: Mar-Nov (b), Apr-Oct (c) and May-Sep (d). The last map shows the differences between the two warmest months, Jul-Aug (e)

heating of the air, while in autumn, the sea is acting as a heat container that makes the autumn cooling slower and hence autumn months warmer than their spring pairs at the coast.

Summer: In all the regions, the warmest summer months are July, August and June in that order. In continental Croatia, the differences in August and July temperatures are less distinct than the differences from June temperatures to those two. In maritime Croatia, the August and July temperatures are almost the same, while the June temperature is 1–2° colder. This change from the continental to maritime temperature regimes of the warmest months can be noticed in *lika* and *moun* Croatia by widening the difference in the June temperature from more similar July and August.

There were several stations with special local characteristics. Station Zagreb-Grič (ID = 38, alt = 157 m) was warmer than other close city stations, showing the urban island temperature effect. Coastal Istrian stations (IDs 24, 102, 117, 120, 122) were warmer than inland ones. The highest station, Zavižan (ID = 41, alt = 1594 m), was already mentioned as the station with the coldest temperatures in Feb. Surprisingly, station Split-Marjan (ID = 32, alt = 122 m), which was

geographically on the southern Adriatic coast, was classified in the neighbouring *hadr* region. We suspect that it could be the influence of the microlocation in elevated city forest, which makes its temperature regime closer to the higher elevation stations of the hinterland (*hadr*).

Next, we present the *grids of monthly temperature climate standard normals for 1981–2010* together with the station data (Fig. 12). The same colour bar for all months allows for insight into the annual course of the mean temperature. The agreement between interpolated and measured values on station locations can be visually confirmed, even though the maps of the normals are aggregated from the time series of monthly grids over the period 1981–2010 and not directly interpolated from the station normals. This means that the interpolation method can reproduce aggregated values such as the means.

The monthly temperature differences between climatological regions based on station normals (Fig. 11) are also confirmed over the grids. For example, subtracting February from the January grid confirms that January was colder than February in continental Croatia (Fig. 13a). Approaching

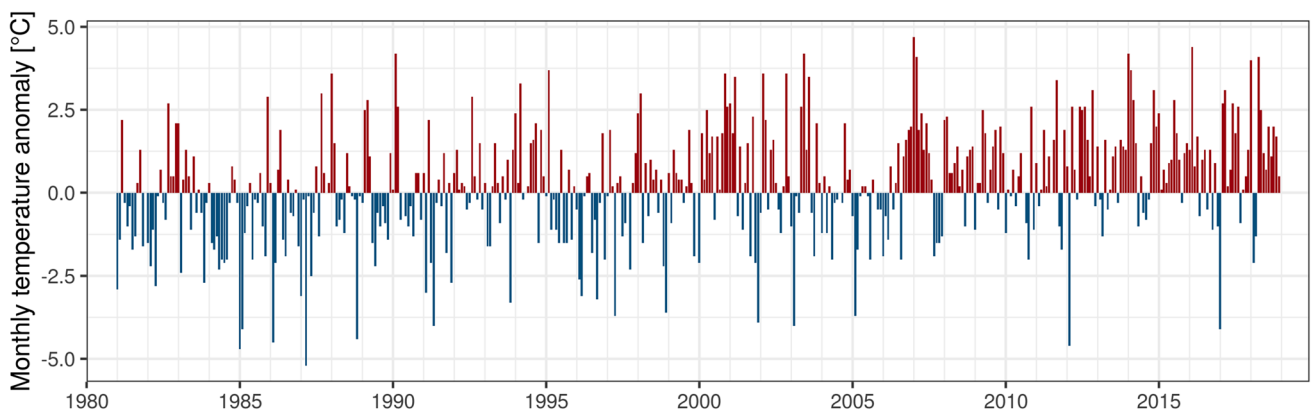


Fig. 14 Time evolution of the monthly temperature anomalies [°C] over the 1981–2018 period averaged for the country. The anomalies were calculated from monthly grids by subtracting the gridded monthly normals for 1981–2010

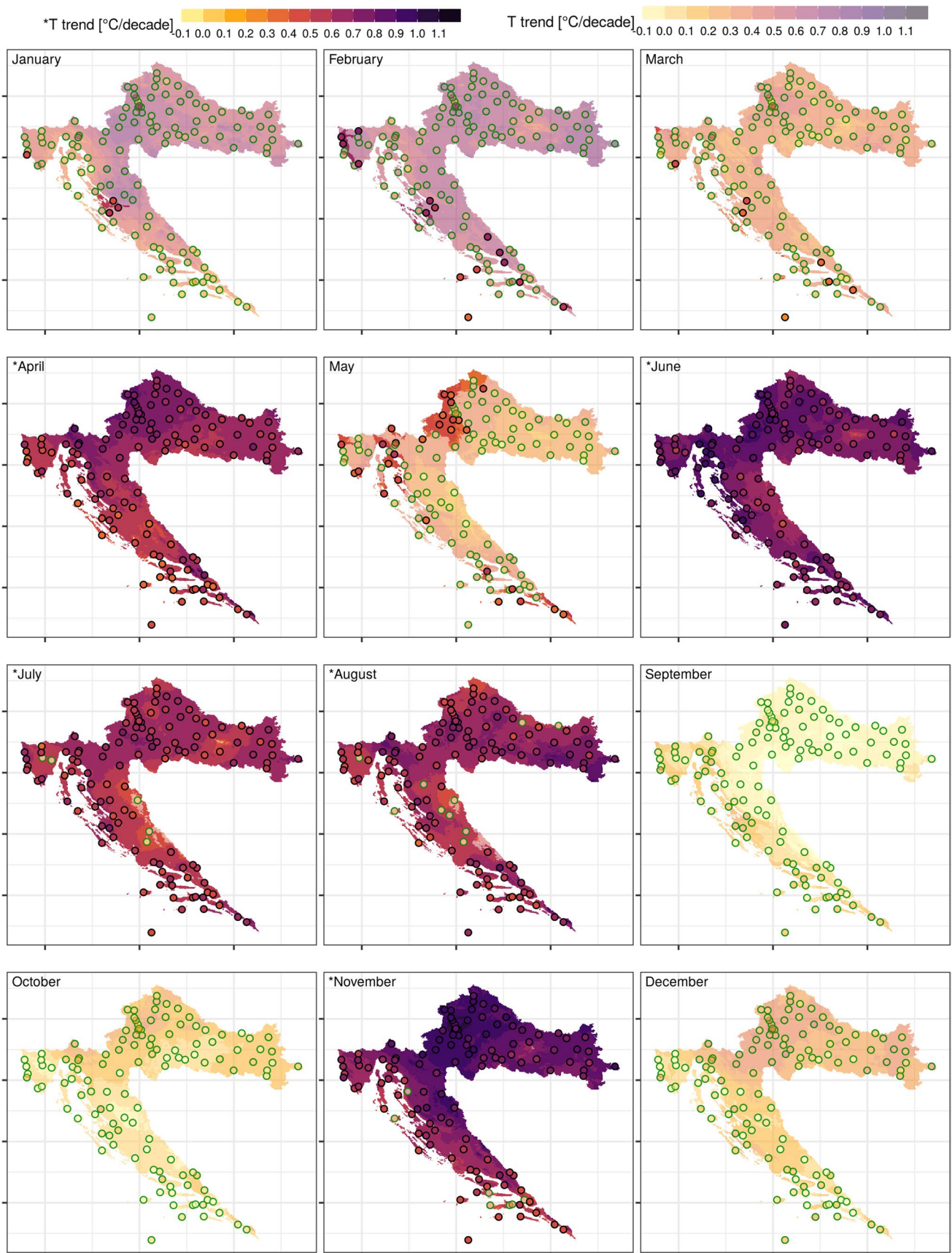


Fig. 15 Monthly temperature trends for the period 1981–2018. The significant trends are presented in full colour (*T trend), while non-significant trends are shown with 50% transparency (T trend). The trends from station data are presented as point symbols for each station. The statistically significant trends are circled with black and the nonsignificant with green colour. Months with dominantly significant trends are marked with an asterisk (*)

the coast, the mean temperature of those two months was becoming more similar. The spring months have similar or slightly warmer temperatures than the autumn months over continental Croatia, which was slightly more pronounced in March, which was up to 1 °C warmer than November (Fig. 13b). However, in the intermittent Lika and mountain region and towards the coast, those differences start to change in favour of warmer autumn months due to the warming effect of the sea. This is pronounced the most in the case of the Apr/Oct pair (Fig. 13c), where October can be 2–3 °C warmer than April on the coast, while over the continent, the differences were smaller. The least pronounced temperature difference was for May/September, where May was slightly warmer in the continent and September at the coast (Fig. 13d). The two warmest months, July and August, have quite similar temperatures at the coast, while July was slightly warmer than August on the continent. This analysis also confirmed the success of the interpolation method to reproduce the spatiotemporal characteristics of the annual cycle of mean monthly temperatures deduced from station data (Fig. 11).

One of the most often used climate monitoring charts is the time evolution of the temperature anomalies calculated from grids and averaged over the regions (Fig. 14). Positive monthly anomalies (red in Fig. 14) were more frequent and lasted over several consecutive months after approximately 2000. The Pettitt test applied to monthly anomalies detected a significant change in the mean in 2000 and an increase of 1 °C in the mean temperature over the later period, indicating the climate change.

Temperature trends based on homogenised monthly temperatures from weather stations give us more detailed insight into this climate change (point symbols in Fig. 15). Positive but nonsignificant warming was observed in January, February and March at most stations. The trend was significant and positive at a few stations in the *nadr* in January (0.5–0.6 °C/decade), at 15 coastal and Adriatic hinterland stations in February (0.5–0.8 °C/decade) and at a few coastal stations in March (0.3–0.5 °C/decade). Positive and significant trends were observed in April (0.4–0.9 °C/decade). In May, all stations experienced positive trends, but they were significant at only several stations, mainly in the *wcon*, *nadr* and *sadr* regions (0.4–0.7 °C/decade). In June, all stations had positive significant trends (0.5–1.0 °C/

decade). In July and August, most of the stations experienced positive significant trends (0.4–0.9 °C/decade), and only a few had positive nonsignificant trends. In September and October, all stations had nonsignificant weak trends. Almost all stations had significant positive trends in November (0.5–1.0 °C/decade). In December, all stations had nonsignificant weak trends.

The overall *annual temperature trend* was positive and significant at all stations (0.3–0.7 °C/decade).

Furthermore, *trends for each calendar month* were calculated from the 38 monthly maps from the 1981–2018 period and presented in Fig. 15 together with the station data. Positive but not always significant trends prevail. Significant strong warming was observed and mapped over the entire Croatian territory in April, June, July, August and November. In *April*, a significant trend of 0.5–0.7 °C/decade was present in *econ* and *ccon* and along the coast and was even stronger in *wcon* and over parts of the *moun* region, where it reaches 0.7–0.9 °C/decade. In *June*, the strongest warming was experienced in *wcon* and over parts of the *moun*, *nadr* and *istr* regions, 0.8–1.0 °C/decade. *Econ* and *ccon* experienced June trends of mostly 0.7–0.8 °C/decade. The *June* trend was 0.5–0.7 °C/decade in continental and southern mountains and in *lika* and 0.7–0.8 °C/decade over the rest of the territory. *July* was warming by 0.4–0.6 °C/decade along the coast, up to 0.6–0.8 °C/decade inland. *August* trends were 0.4–0.6 °C/decade in *lika*, 0.5–0.7 °C/decade along the coast, 0.6–0.8 in *moun*, *wcon* and *ccon* and up to 0.9 °C/decade in *econ* region. The July and August maps look similar, but there was noticeably stronger warming during August in the continental regions. The strongest significant trends are measured and mapped in *November*. The strongest trends were around the capital of Zagreb, reaching 1.0–1.1 °C/decade. The rest of the *wcon* was experiencing a trend of 0.9–1.0 °C/decade. The *ccon* and *econ* were warming by 0.8–0.9 °C/decade, slightly slower over eastern continental mountains. The main mountain Dinaric region that separates the continental part of the country from the Adriatic was warming by 0.7–0.9 °C/decade, while the coast was warming by 0.5–0.7 °C/decade. In *May*, only the western continental region and smaller parts along the coast experienced a significant trend of 0.3–0.5 °C/decade. The measured amount, sign and significance of trends estimated at meteorological stations (point symbols in Fig. 15) were accurately captured on the trend maps calculated from the monthly maps.

Finally, the mean annual temperature for the normal period 1981–2010 was calculated from the monthly normals (Fig. 16a); then, annual anomalies were calculated as differences of each annual grid and the annual normal (Fig. 16b) and spatially aggregated over Croatia, while the annual trend was calculated from the 38 mean annual temperature grids (Fig. 16c). Each annual grid was calculated as the mean from the corresponding monthly grids. *The annual temperature*

climate standard normal for 1981–2010 in Croatia ranges from 1 °C on the highest Croatian mountain Dinara to 17 °C in the southern Adriatic (Fig. 16a). *Annual anomalies* were dominantly positive from 1999, up to 1.4 °C (Fig. 16b). After 1999, only 2004, 2005 and 2010 were colder than average, with 2005 being noticeably colder (for 0.7 °C). The Pettitt test applied to annual anomalies detected a significant change in 1998, with the same amount of 1 °C of the temperature increase as calculated from the monthly anomalies. *Annual temperature trends* were the highest in the capital of Zagreb and its surroundings, above 0.6 °C/decade (Fig. 16c). The rest of this western continental region, the large part of the northern mountainous region, the most eastern continental region and the farthest southern Dalmatia experience strong temperature trends of 0.5–0.6 °C/decade. The central continental region, Istria, Lika, the southern mountainous region and most of the Adriatic coast exhibit a trend of 0.4–0.5 °C/decade. There were regions in the Adriatic hinterland and southern Adriatic with trends below 0.4 °C/decade.

6 Discussion and conclusions

This study presents the most extensive set of monthly homogenised station data and the first set of monthly grids at a 1 km spatial resolution suitable for climate monitoring in Croatia. Well-known homogenisation and interpolation methods have been applied in the study, with the extensive analysis and optimisation of the parameters for both methods.

Homogenisation could not be supported by the digitised metadata, so conservative SNHT critical levels were used

to avoid oversmoothing the observed monthly temperatures. They were higher than those suggested in Khaliq and Ouarda (2007), who derived the critical SNHTs from synthetic white noise series. Climatological anomalies will show some degree of station autocorrelation, spatial cross-correlation and local or general trends depending on the type of climatic variable, its spatial variability, the density of the observing network and the temporal scale of the data (Mamara et al. 2013; Guijarro 2021; Willett et al. 2014). That is why the default SNHT thresholds in the *climatol* are higher than those obtained in Khaliq and Ouarda (2007). We compared the *climatol* visualisation outputs, breaks and derived trends for several SNHT1 and SNHT2 combinations, resulting in higher than default SNHT thresholds, similar to Curci et al. (2021) and Meseguer-Ruiz et al. (2018). Compared to our preliminary homogeneity study (Nimac and Perčec Tadić 2017), approximately 40% of the breaks identified there were in the same year or even month as the breaks detected in this study. We were able to compare the proposed breaks of homogeneity (Appendix) with the breaks and paper metadata for 22 stations documented in Pandžić and Likso (2010). We found that most of the abrupt breaks are successfully detected in both studies, while the differences could be due to a more general version of SNHT in Pandžić and Likso (2010), which detects artificial linear trends in temperature series in addition to abrupt breaks. The remaining differences can be due to different periods and SNHT critical values and annual time scales in Pandžić and Likso (2010) compared to monthly values in the present study.

Regarding homogenisation, negative adjustments over the climate regions agree with the negative adjustment reported for E-OBS (Squintu et al. 2019). However, the sizes of the adjustments with median values of -0.5–0.0 °C were larger

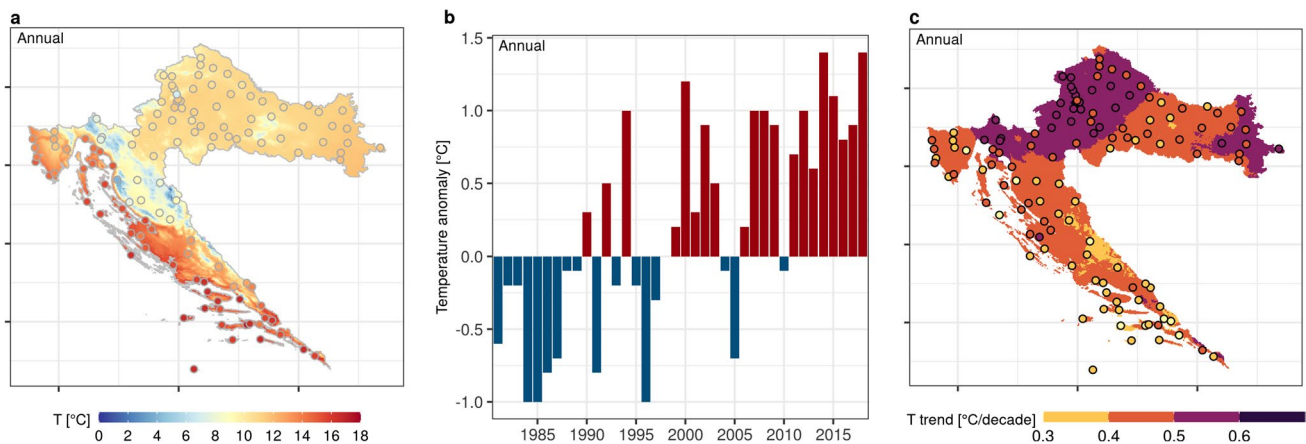


Fig. 16 Mean annual temperature for the period 1981–2010 calculated from the mean monthly grids (a). Temporal evolution of the temperature anomalies from 1981–2010 normal, spatially averaged

over the country (b). Annual temperature trend for the period 1981–2018 calculated from the annual grids (c)

than in Squintu et al. (2019) who assessed the statistical performance of the homogenisation using all the data. In our research, ME and RMSE (Fig. 5) were calculated only from the data corrected due to homogenisation resulting in larger, but we believe more objective estimates of the adjustments.

Monthly grids were accompanied by *normalised error maps* that provide an estimate of accuracy. Parts of the maps with normalised errors above 0.4 were considered less accurate, which was observed in isolated elevated regions without observations available.

Maps of monthly and annual climate standard normals and trends were calculated from the time series of monthly grids. Another approach to calculate such a product would be an interpolation of the station values of the normal or trend. However, with interpolated monthly values of the temperature, we were able to reproduce the normals and trends of the monthly and annual temperatures comparable to those calculated from station data. The interpolation procedure reproduced the spatial characteristics of colder January than February over the continental regions, warmer spring than autumn months in the continental regions, warmer autumn than spring months in the intermittent and coastal regions and warmer July than August inland (Fig. 13), the characteristics that were also observed from the station data (Fig. 11).

The months with significant positive trends in temperature, that is, April, June, July, August and November, experience *stronger trends over continental and mountainous regions compared to the coast* (Fig. 15). The established land/sea warming ratio of 1.3–1.4 over Croatia follows the global land/sea warming ratio (Sutton et al. 2007), which is in the range of 1.36–1.84, independent of global mean temperature change. Intuitive and older theories would explain this difference by the smaller heat capacity of soil, which as a consequence heats more rapidly. Manabe et al. (1991) questioned this and pointed out that over the oceans, air can cool down by evaporation at the sea surface, while over the land, the moisture content was constrained, so the warming becomes stronger. In dry air, more sensible heat warms the air, slowing cloud formation and enhancing further drying and consequently more heating. More recent theories would rely more on moisture and energy balance examined by several climate models (Sutton et al. 2007). Joshi et al. (2008) examined a large ensemble of climate model integrations and showed that the land/sea contrast in equilibrium but also in transient radiation simulations was associated with local feedbacks such as different changes in the temperature lapse rate over land and sea and the change in a hydrological cycle over land, rather than with externally imposed radiative forcing. The context for interpreting equilibrium climate sensitivity (ECT) and transient climate response (TCR) from the CMIP6 Earth system models is presented in detail in Meehl et al. (2020).

Elevation-dependent warming (EDW) is another observed feature of global climate change, and there is evidence for it over the Alps, Rockies, and the Tibetan Plateau, all of which are in the mid-latitudes (Miller et al. 2021). Pepin et al. (2015) concluded that there is evidence that many, but not all, mountain ranges show enhanced warming with elevation. Higher elevation stations in Croatia (between 750 and 1594 m) showed significant warming annual and summer trends, but similar and even stronger trends are found at lower elevation stations. A similar absence of EDW was also observed over close regions of the mid-latitude eastern Italian Alps (Tudoroiu et al. 2016).

The highest annual trend (0.67 °C/decade) in the capital of Zagreb is not just a result of climate change but also *urbanisation*. Nimac et al. (2021) observed a strong increase in the number of summer days (9 days/decade), while the number of tropical nights increased by 8 days/decade during the period 1990–2019. Consequently, the summer months are going to be more uncomfortable for citizens.

Annual trends of 0.3–0.7 °C/decade are significant for the entire country. They are stronger than the trends of 0.26 °C/decade over the Pannonian Basin for 1970–2005 from the E-OBS (Table 2 in Lazić et al. 2021), probably due to the temperature rise after 2005. They are comparable with annual trends of approximately 0.4°/decade for the 1980–2019 period for the Abruzzo region in central Italy (Curci et al. 2021), where a similar approach is used for homogenisation of the data series. It seems that the observed trends over the Mediterranean are 2–2.5 times stronger than the global mean warming, especially during summer (van Oldenborgh et al. 2009). Serious warnings come from the climate model results, which predict that the Mediterranean region is likely to warm at a rate approximately 20% larger than the global annual mean surface temperature (Lionello and Scarascia 2018). The values are particularly high in summer and in the continental areas north of the basin, where warming will generally be 50% stronger than at the global scale and locally even twice as large (Lionello and Scarascia 2018). The region will face consequences such as devastating heatwaves, water shortages, loss of biodiversity and risks to food production.

The *monthly anomalies* from the 1981–2010 average for Croatia (Fig. 14) are comparable with the temperature anomalies¹ over Europe derived from ERA-Interim reanalysis data (substituted later by ERA5 (Hersbach et al. 2020)) and provided by the Copernicus Climate Change Service. Anomalies for April, June, July, August and November (not shown) were mostly strong and positive from the beginning of the twenty-first century, which is related to already

¹ C3S temperature anomaly for Europe.

discussed significant positive trends in station data over the entire country in those months (Fig. 15).

Even though the presented analysis is based on data for a limited area, we believe that the methodology is useful for the development of any similar research and climate monitoring products. We presented the power of *clustering* in defining the nine Croatian climate regions and showed how *homogenisation* affects the trends in the data. Additionally, we highlighted the importance of objectively estimating the parameters of local neighbourhoods for kriging and showed, at least for Croatia, that a single set of these parameters can be used for all months with a negligible increase in the RMSE.

The *monthly maps* are produced for the period 1981–2018 together with the error estimates. Looking at the aggregated statistical values derived from the monthly maps, it was confirmed that the interpolation method can successfully reproduce the means (Fig. 12 and Fig. 16a), annual cycle differences (Fig. 13) and trends (Fig. 15 and Fig. 16c). The maps were used further to derive the monthly anomalies.

This study presents the last four decades of mean air temperature and its change over Croatia, pointing to *prevailing*

positive annual anomalies in the twenty-first century and strong and significant warming trends. From the beginning of the twenty-first century, average monthly anomalies are often positive and up to 4.7 °C (January 2007) warmer than the average and only occasionally negative (Fig. 14). The measured amount, sign and significance are accurately captured on the trend maps calculated from the monthly maps (Fig. 15). The significant strong warming of 0.3–1.0 °C/decade was observed and mapped over the entire Croatian territory in April, June, July, August and November together with the significant annual trends of 0.3–0.7 °C/decade (Fig. 16c) that were stronger inland than on the coast. The EDW was not confirmed for Croatian Dinarides.

The new monthly temperature grids belong to the developing *CroMonthlyGrids* dataset that is intended to support climate monitoring, climate change detection and adaptation planning on national and local administrative levels. Further grids are in preparation for minimum and maximum temperatures and monthly precipitation. These grids will form the basis for the calculation of climate normals and operational national climate monitoring products with further applications in sectors such as hydrology, forestry, agronomy or health.

Appendix

Table 2 Spatiotemporal inventory of detected homogeneity breaks. The columns denote a region, station identifier (ID), station name (Station), start and end of the data available in the relational database,

percentage of original (OR), interpolated (IN) and homogenised (HO) data in the final series and time of the breaks (brk1 to brk3) with the SNHT value in brackets

Region	ID	Station	Start	End	OR	IN	HO	brk1	brk2	brk3
econ	8	Gradište	1981–01	2018–12	58	-	42	1996–11 (118)	-	-
econ	19	Osijek	1981–01	2018–12	99	1	-	-	-	-
econ	20	Osijek - Klisa aerodrom	1981–01	2018–12	45	29	26	2002–02 (50.5)	-	-
econ	53	Brestovac Belje	1981–01	2018–12	83	17	-	-	-	-
econ	63	Donji Miholjac	1981–01	2018–12	100	-	-	-	-	-
econ	66	Đakovo	1981–01	2018–12	96	4	-	-	-	-
econ	72	Ilok	1981–01	2018–12	73	27	-	-	-	-
econ	143	Valpovo - Tiborjanci	1981–01	2018–12	63	5	32	1994–12 (40.4)	-	-
econ	145	Vinkovci	1981–01	2014–05	86	14	-	-	-	-
econ	158	Županja	1981–01	2018–12	80	20	-	-	-	-
ccon	3	Daruvar	1981–01	2018–12	59	-	41	1996–09 (163.2)	-	-
ccon	31	Slavonski Brod	1981–01	2018–12	100	0	-	-	-	-
ccon	35	Varaždin	1981–01	2018–12	100	-	-	-	-	-
ccon	58	Čakovec	1981–01	2018–12	92	6	2	2018–04 (40.7)	-	-
ccon	67	Đurđevac	1981–01	2018–12	100	-	-	-	-	-
ccon	71	Hrvatska Kostajnica	1981–01	2018–12	77	23	-	-	-	-
ccon	78	Koprivnica	1981–01	2018–12	43	0	57	2011–01 (85.1)	2012–10 (48.3)	-
ccon	85	Kutina	1981–01	2018–12	73	27	-	-	-	-
ccon	91	Lipik	1981–01	2018–12	50	19	31	2000–06 (153.1)	-	-
ccon	94	Ludbreg - Hrastovsko	1981–01	2018–12	21	1	78	2011–04 (42.6)	-	-
ccon	99	Našice	1981–01	2018–12	93	7	-	-	-	-
ccon	100	Nova Gradiška - Cernik	1981–01	2018–12	57	15	27	1996–12 (50.2)	-	-

Table 2 (continued)

Region	ID	Station	Start	End	OR	IN	HO	brk1	brk2	brk3
ccon	103	Novi Marof	1981-01	2018-12	56	7	37	1997-02 (45.3)	-	-
ccon	104	Novska	1981-01	2018-12	73	27	-	-	-	-
ccon	106	Opeke	1981-01	2007-06	13	31	56	2002-08 (39)	-	-
ccon	118	Požega	1981-01	2018-12	41	21	38	1992-12 (62.7)	2005-11 (73.5)	-
ccon	127	Slatina - Medinci	1981-01	2018-12	61	3	36	1995-11 (89.6)	-	-
ccon	135	Sunja	1981-01	2018-12	37	1	62	2005-02 (94.5)	-	-
ccon	146	Virovitica	1981-01	2018-12	69	31	-	-	-	-
ccon	147	Voćin	1981-01	2018-12	48	9	44	2000-05 (86.6)	-	-
wcon	1	Bilogora	1981-01	2018-12	98	2	-	-	-	-
wcon	2	Bjelovar	1981-01	2018-12	38	-	62	1988-11 (35.4)	1998-10 (35.4)	2004-07 (37.2)
wcon	10	Karlovac	1981-01	2018-12	46	-	54	1993-01 (48.3)	2001-08 (56.4)	-
wcon	13	Krapina	1993-09	2018-12	67	33	-	-	-	-
wcon	14	Križevci	1981-01	2018-12	50	-	50	2001-02 (110.7)	-	-
wcon	18	Ogulin	1981-01	2018-12	100	-	-	-	-	-
wcon	30	Sisak	1981-01	2018-12	87	2	12	1985-07 (45.1)	-	-
wcon	38	Zagreb - Grič	1981-01	2018-12	100	-	-	-	-	-
wcon	39	Zagreb - Maksimir	1981-01	2018-12	73	-	27	1991-06 (122.1)	-	-
wcon	40	Zagreb - Pleso aerodrom	1981-01	2018-12	99	1	-	-	-	-
wcon	50	Bosiljevo	1981-01	2018-12	74	0	26	1984-01 (40.8)	1990-12 (75.9)	-
wcon	59	Čazma	1981-01	2018-12	58	3	39	1987-03 (72.9)	1996-09 (38)	-
wcon	74	Jastrebarsko	1981-01	2014-07	84	16	-	-	-	-
wcon	105	Oborovo	1986-01	2018-12	44	14	43	2002-06 (57.4)	-	-
wcon	112	Petrinja	1981-01	2018-12	27	20	53	2008-05 (73.2)	-	-
wcon	113	Pisarovina	1981-01	2018-12	58	4	39	1995-11 (41)	-	-
wcon	119	Pregrada	1992-02	2018-12	70	30	-	-	-	-
wcon	123	Samobor	1981-01	2018-12	11	5	84	1987-03 (43.6)	2014-12 (74.5)	-
wcon	128	Slunj	1981-01	2018-12	87	13	-	-	-	-
wcon	133	Stubičke Toplice	1981-01	2018-12	92	8	-	-	-	-
wcon	138	Sv. Ivan Zelina	1981-01	2018-12	85	15	-	-	-	-
wcon	141	Topusko	1981-01	2018-12	56	20	25	1990-12 (44.4)	-	-
wcon	151	Lekenik	1981-01	2018-12	21	3	76	2011-02 (86)	-	-
wcon	154	Zabok	1991-05	2018-12	72	28	-	-	-	-
wcon	155	Zagreb - Botinec	1981-01	2014-12	41	11	48	1988-11 (39.1)	2000-05 (44.7)	-
wcon	156	Zagreb - Rim	1981-02	2018-12	98	2	-	-	-	-
lika	7	Gospić	1981-01	2018-12	58	-	42	1996-11 (47.5)	-	-
lika	62	Donji Lapac	1982-06	2018-12	50	29	21	1999-11 (37.5)	-	-
lika	70	Gračac	1981-01	2018-12	69	14	16	1987-03 (102)	-	-
lika	80	Korenica	1981-01	2018-12	82	18	-	-	-	-
lika	90	Ličko Lešće	1981-01	2018-12	100	-	-	-	-	-
lika	93	Lovinac	1981-01	2018-12	73	27	-	-	-	-
moun	21	Parg	1981-01	2018-12	100	-	-	-	-	-
moun	25	Puntijarka	1981-01	2018-12	97	3	-	-	-	-
moun	41	Zavižan	1981-01	2018-12	97	3	-	-	-	-
moun	44	Baške Oštarije	1981-01	2010-10	73	27	-	-	-	-
moun	92	Lokve Brana	1981-01	2015-11	83	8	9	1984-05 (47.4)	-	-
moun	149	Vrelo Ličanke	1981-01	2018-12	100	-	-	-	-	-
istr	22	Pazin	1981-01	2018-12	100	-	-	-	-	-
istr	24	Pula	1981-01	2018-12	61	1	38	1995-08 (88.3)	-	-
istr	42	Abrami	1981-01	2017-02	28	5	67	2006-08 (39.2)	-	-
istr	51	Botonega	1987-05	2018-12	37	17	46	2004-11 (104.4)	-	-

Table 2 (continued)

Region	ID	Station	Start	End	OR	IN	HO	brk1	brk2	brk3
istr	60	Čepić	1981-01	2018-12	97	3	-	-	-	-
istr	102	Novigrad - Celega	1982-05	2012-01	75	25	-	-	-	-
istr	117	Poreč	1981-01	2018-12	69	2	29	1992-09 (95.8)	-	-
istr	120	Pula - aerodrom	1981-01	2018-12	95	5	-	-	-	-
istr	122	Rovinj	1981-01	2018-12	80	4	15	1988-06 (59)	-	-
hadr	11	Knin	1981-01	2018-12	100	0	-	-	-	-
hadr	32	Split - Marjan	1981-01	2018-12	100	-	-	-	-	-
hadr	65	Drniš	1981-01	2018-12	85	15	-	-	-	-
hadr	73	Imotski	1981-01	2018-12	100	0	-	-	-	-
hadr	84	Kuna	1981-01	2018-12	78	-	22	1989-07 (40.4)	-	-
hadr	121	Ričice - Brana	1993-01	2018-12	68	32	-	-	-	-
hadr	126	Sinj	1981-01	2018-12	53	0	47	1998-10 (41.4)	-	-
hadr	139	Šestanovac	1981-01	2018-12	5	2	93	1989-05 (44.2)	2017-01 (47.3)	-
hadr	150	Vrgorac	1981-01	2018-12	16	10	74	1998-09 (104.2)	2014-03 (35)	-
nadr	17	Mali Lošinj	1981-01	2018-12	97	3	-	-	-	-
nadr	26	Rab	1981-01	2018-12	97	3	-	-	-	-
nadr	27	Rijeka	1981-01	2018-12	100	-	-	-	-	-
nadr	28	Rijeka - aerodrom	1981-01	2018-12	77	23	-	-	-	-
nadr	29	Senj	1981-01	2018-12	100	-	-	-	-	-
nadr	34	Šibenik	1981-01	2018-12	54	3	44	1997-08 (82.5)	-	-
nadr	36	Zadar	1981-01	2018-12	100	-	-	-	-	-
nadr	37	Zadar - aerodrom	1981-01	2018-12	90	10	-	-	-	-
nadr	48	Biograd na moru	1981-01	2018-12	87	3	11	1985-04 (38.2)	-	-
nadr	55	Cres	1981-01	2018-12	100	-	-	-	-	-
nadr	56	Crikvenica	1981-01	2018-12	30	2	68	1991-10 (57.5)	1997-03 (57.1)	2011-03 (46.7)
nadr	81	Krk	1981-01	2018-12	67	33	-	-	-	-
nadr	101	Novigrad	1981-01	2018-12	81	19	-	-	-	-
nadr	110	Pag	1981-01	2018-12	25	4	71	1989-02 (35.5)	2002-10 (42.9)	2009-06 (47.2)
nadr	124	Sestrice Vele	1981-01	2018-12	100	-	-	-	-	-
nadr	125	Silba	1981-01	2018-12	96	4	-	-	-	-
nadr	130	Starigrad - Paklenica	1992-04	2018-07	68	32	-	-	-	-
nadr	137	Sv. Ivan na Pučini	1984-02	2018-12	88	12	-	-	-	-
sadr	4	Dubrovnik	1981-01	2018-12	100	-	-	-	-	-
sadr	5	Dubrovnik - aerodrom	1981-01	2018-12	62	9	28	1993-10 (50.3)	-	-
sadr	9	Hvar	1981-01	2018-12	100	-	-	-	-	-
sadr	12	Komiža	1981-01	2018-12	37	2	61	2005-02 (108.4)	-	-
sadr	15	Lastovo	1981-01	2018-12	100	-	-	-	-	-
sadr	16	Makarska	1981-01	2018-12	36	7	57	2012-03 (37.1)	-	-
sadr	23	Ploče	1981-01	2018-12	100	-	-	-	-	-
sadr	33	Split - aerodrom	1981-01	2018-12	98	2	-	-	-	-
sadr	49	Bol	1981-02	2018-12	28	19	52	2008-04 (45.7)	-	-
sadr	69	Govedari klim	1981-01	2018-12	96	4	-	-	-	-
sadr	75	Jelsa	1981-01	2018-12	96	4	-	-	-	-
sadr	79	Korčula	1981-01	2018-12	62	2	36	1995-06 (43.6)	-	-
sadr	107	Opuzen	1981-01	2018-12	27	4	69	2008-02 (43.5)	-	-
sadr	108	Orebić	1981-01	2012-02	77	23	-	-	-	-
sadr	111	Palagruža	1981-01	2018-12	91	9	-	-	-	-
sadr	131	Ston	1981-01	2018-11	58	17	25	2000-07 (64.7)	2006-06 (56.8)	-
sadr	136	Sutivan	1981-01	2018-12	26	3	70	2008-02 (66)	-	-
sadr	144	Vela Luka	1981-01	2018-12	96	4	-	-	-	-

Supplementary Information The online version contains supplementary material available at <https://doi.org/10.1007/s00704-022-04241-y>.

Acknowledgements The authors acknowledge the time and effort devoted by the two anonymous reviewers which helped to improve this paper. MPT thanks her PhD supervisor Tomislav Hengl for continuous support.

Author contribution Melita Perčec Tadić developed the study concept, created the R-code used in the study, performed data analysis and wrote the first version of the manuscript. Zoran Pasarić and Jose A. Guijarro modified and commented on further versions of the study design and the manuscript. All authors read and approved the final version of the manuscript.

Funding Research of MPT was supported by employer, Croatian Meteorological and Hydrological Service, and by the project UKV – Carstic Coastal Water Management Endangered by Climate Changes (KK.05.1.1.02.0022). Open access funding is provided by Croatian Meteorological and Hydrological Service.

Data availability Original station data are the property of the Croatian Meteorological and Hydrological Service. They are available from the corresponding author on reasonable request. Homogenised station data series, metadata of the stations and monthly temperature grids are from the corresponding author on reasonable request.

Code availability Code is available upon reasonable request.

Declarations

Ethics approval Not applicable.

Consent to participate Not applicable.

Consent for publication Not applicable.

Competing interests The authors declare no competing interests.

Open Access This article is licensed under a Creative Commons Attribution 4.0 International License, which permits use, sharing, adaptation, distribution and reproduction in any medium or format, as long as you give appropriate credit to the original author(s) and the source, provide a link to the Creative Commons licence, and indicate if changes were made. The images or other third party material in this article are included in the article's Creative Commons licence, unless indicated otherwise in a credit line to the material. If material is not included in the article's Creative Commons licence and your intended use is not permitted by statutory regulation or exceeds the permitted use, you will need to obtain permission directly from the copyright holder. To view a copy of this licence, visit <http://creativecommons.org/licenses/by/4.0/>.

References

- Alexandersson H, Moberg A (1997) Homogenization of Swedish temperature data. Part I: Homogeneity Test for Linear Trends. *Int J Climatol* 17:25–34. [https://doi.org/10.1002/\(SICI\)1097-0088\(199701\)17:1%3c25::AID-JOC103%3e3.0.CO;2-J](https://doi.org/10.1002/(SICI)1097-0088(199701)17:1%3c25::AID-JOC103%3e3.0.CO;2-J)
- Beaulieu C, Seidou O, Ouarda T, Zhang X, Boulet G, Yagouti A (2008) Intercomparison of homogenization techniques for precipitation data. *Water Resour Res* 440. <https://doi.org/10.1029/2006WR005615>
- Brinckmann S, Kraehenmann S, Bissolli P (2016) High-resolution daily gridded data sets of air temperature and wind speed for Europe. *Earth Syst Sci Data* 8:491–516. <https://doi.org/10.5194/essd-8-491-2016>
- Burrough PA, McDonnell R, Burrough PA (1998) Principles of geographical information systems. Oxford University Press, Oxford, New York
- Coll J, Domonkos P, Guijarro J, Curley M, Rustemeier E, Aguilar E, Walsh S, Sweeney J (2020) Application of homogenization methods for Ireland's monthly precipitation records: comparison of break detection results. *Int J Climatol* 40:6169–6188. <https://doi.org/10.1002/joc.6575>
- Curci G, Guijarro JA, Antonio LD, Bacco MD, Lena BD, Scorzini AR (2021) Building a local climate reference dataset: application to the Abruzzo region (Central Italy), 1930–2019. *Int J Climatol* n/a:23. <https://doi.org/10.1002/joc.7081>
- Domonkos P (2021) Combination of using pairwise comparisons and composite reference series: a new approach in the homogenization of climatic time series with ACMANT. *Atmosphere* 12:1134. <https://doi.org/10.3390/atmos12091134>
- Domonkos P, Guijarro JA, Venema V, Brunet M, Sigró J (2021) Efficiency of time series homogenization: method comparison with 12 monthly temperature test datasets. *J Clim* 34:2877–2891. <https://doi.org/10.1175/JCLI-D-20-0611.1>
- Draper NR, Smith H (1998) Applied regression analysis, 3rd edn. Wiley, New York
- Evans JS (2020) spatialEco-package. R package version 1.3–1. <https://github.com/jeffrejevans/spatialEco>. Accessed 22 Aug 2021
- Fick SE, Hijmans RJ (2017) WorldClim 2: new 1-km spatial resolution climate surfaces for global land areas. *Int J Climatol* 37:4302–4315. <https://doi.org/10.1002/joc.5086>
- Frei C, Schär C (1998) A precipitation climatology of the Alps from high-resolution rain-gauge observations. *Int J Climatol* 18:873–900. [https://doi.org/10.1002/\(SICI\)1097-0088\(19980630\)18:8%3c873::AID-JOC255%3e3.0.CO;2-9](https://doi.org/10.1002/(SICI)1097-0088(19980630)18:8%3c873::AID-JOC255%3e3.0.CO;2-9)
- Gräler B, Pebesma E, Heuvelink G (2016) Spatio-Temporal Interpolation Using Gstat R J 8:204–218
- Guijarro JA (2019) Package 'climatol' Version 3.1.2. <https://cran.r-project.org/web/packages/climatol/climatol.pdf>. Accessed 23 Oct 2020
- Guijarro JA (2021) Homogenization of climatic series with Climatol Version 3.1.1. http://www.climatol.eu/homog_climatol-en.pdf. Accessed 23 Oct 2020
- Haylock MR, Hofstra N, Klein Tank AMG, Klok EJ, Jones PD, New M (2008) A European daily high-resolution gridded data set of surface temperature and precipitation for 1950–2006. *J Geophys Res* 113:D20119. <https://doi.org/10.1029/2008JD010201>
- Hengl T (2009) A practical guide to geostatistical mapping. University of Amsterdam
- Hengl T, Heuvelink GBM, Stein A (2004) A generic framework for spatial prediction of soil variables based on regression-kriging. *Geoderma* 120:75–93. <https://doi.org/10.1016/j.geoderma.2003.08.018>
- Hengl T, Heuvelink G, Rossiter D (2007) About regression-kriging: from equations to case studies. *Comput Geosci* 33:1301–1315. <https://doi.org/10.1016/j.cageo.2007.05.001>
- Hengl T, Heuvelink GBM, Stein A (2003) Comparison of kriging with external drift and regression-kriging. Technical note. ITC. https://webapps.itc.utwente.nl/librarywww/papers_2003/misca/hengl_comparison.pdf. Accessed 9 Jan 2022
- Hersbach H, Bell B, Berrisford P, Hirahara S, Horányi A, Muñoz-Sabater J, Nicolas J, Peubey C, Radu R, Schepers D, Simmons A, Soci C, Abdalla S, Abellan X, Balsamo G, Bechtold P, Biavati G, Bidlot J, Bonavita M, Chiara GD, Dahlgren P, Dee D, Diamantakis M, Dragani R, Flemming J, Forbes R, Fuentes M, Geer A, Haimberger L, Healy S, Hogan RJ, Hólm E, Janisková M, Keeley

- S, Laloyaux P, Lopez P, Lupu C, Radnoti G, de Rosnay P, Rozum I, Vamborg F, Villaume S, Thépaut J-N (2020) The ERA5 global reanalysis. *Q J R Meteorol Soc* 146:1999–2049. <https://doi.org/10.1002/qj.3803>
- Hiebl J, Auer I, Böhm R, Schöner W, Maugeri M, Lentini G, Spinoni J, Brunetti M, Nanni T, Perčec Tadić M, Bihari Z, Dolinar M, Müller-Westermeier G (2009) A high-resolution 1961–1990 monthly temperature climatology for the greater Alpine region. *Meteorol Z* 18:507–530. <https://doi.org/10.1127/0941-2948/2009/0403>
- Hiemstra PH, Pebesma EJ, Twenhöfel CJW, Heuvelink GBM (2009) Real-time automatic interpolation of ambient gamma dose rates from the Dutch radioactivity monitoring network. *Comput Geosci* 35:1711–1721. <https://doi.org/10.1016/j.cageo.2008.10.011>
- Hijmans RJ, Cameron SE, Parra JL, Jones PG, Jarvis A (2005) Very high resolution interpolated climate surfaces for global land areas. *Int J Climatol* 25:1965–1978. <https://doi.org/10.1002/joc.1276>
- Hijmans RJ (2020) raster: geographic data analysis and modeling. R package. <https://CRAN.R-project.org/package=raster>. Accessed 22 Aug 2021
- Hofstra N, Haylock M, New M, Jones P, Frei C (2008) Comparison of six methods for the interpolation of daily, European climate data. *J Geophys Res Atmospheres* 113. <https://doi.org/10.1029/2008JD010100>
- Hudson G, Wackernagel H (1994) Mapping temperature using kriging with external drift: theory and an example from Scotland. *Int J Climatol* 14:77–91. <https://doi.org/10.1002/joc.3370140107>
- IPCC (2021) IPCC Summary for Policymakers. In: Climate Change 2021: The Physical Science Basis. Contribution of Working Group I to the Sixth Assessment Report of the Intergovernmental Panel on Climate Change [Masson-Delmotte, V., P. Zhai, A. Pirani, S. L. Connors, C. Péan, S. Berger, N. Caud, Y. Chen, L. Goldfarb, M. I. Gomis, M. Huang, K. Leitzell, E. Lonnoy, J.B.R. Matthews, T. K. Maycock, T. Waterfield, O. Yelekçi, R. Yu and B. Zhou (eds.)]. In Press
- Joshi MM, Gregory JM, Webb MJ, Sexton DMH, Johns TC (2008) Mechanisms for the land/sea warming contrast exhibited by simulations of climate change. *Clim Dyn* 30:455–465. <https://doi.org/10.1007/s00382-007-0306-1>
- Khaliq MN, Ouarda TBMJ (2007) On the critical values of the standard normal homogeneity test (SNHT). *Int J Climatol* 27:681–687. <https://doi.org/10.1002/joc.1438>
- Knotters M, Brus DJ, Oude Voshaar JH (1995) A comparison of kriging, co-kriging and kriging combined with regression for spatial interpolation of horizon depth with censored observations. *Geoderma* 67:227–246. [https://doi.org/10.1016/0016-7061\(95\)00011-C](https://doi.org/10.1016/0016-7061(95)00011-C)
- Kolendowicz L, Czernecki B, Pórolniczak M, Taszarek M, Tomczyk AM, Szyga-Pluga K (2019) Homogenization of air temperature and its long-term trends in Poznań (Poland) for the period 1848–2016. *Theor Appl Climatol* 136:1357–1370. <https://doi.org/10.1007/s00704-018-2560-z>
- Lazić I, Tošić M, Djurdjević V (2021) Verification of the EURO-CORDEX RCM Historical Run Results over the Pannonian Basin for the Summer Season. *Atmosphere* 12:714. <https://doi.org/10.3390/atmos12060714>
- Li J, Heap A (2014) Spatial interpolation methods applied in the environmental sciences: a review. *Env Model Softw*. <https://doi.org/10.1016/j.envsoft.2013.12.008>
- Likso T (2003) Inhomogeneities in temperature time series in Croatia. *Croat Meteorol J* 38:3–9
- Lionello P, Scarascia L (2018) The relation between climate change in the Mediterranean region and global warming. *Reg Environ Change* 18:1481–1493. <https://doi.org/10.1007/s10113-018-1290-1>
- Lionello P, Scarascia L (2020) The relation of climate extremes with global warming in the Mediterranean region and its north versus south contrast. *Reg Environ Change* 20:31. <https://doi.org/10.1007/s10113-020-01610-z>
- Mamara A, Argiriou AA, Anadranistakis M (2013) Homogenization of mean monthly temperature time series of Greece. *Int J Climatol* 33:2649–2666. <https://doi.org/10.1002/joc.3614>
- Manabe S, Stouffer RJ, Spelman MJ, Bryan K (1991) Transient responses of a coupled ocean–atmosphere model to gradual changes of atmospheric CO₂. Part I. Annual Mean Response *J Clim* 4:785–818. [https://doi.org/10.1175/1520-0442\(1991\)004%3c0785:TROACO%3e2.0.CO;2](https://doi.org/10.1175/1520-0442(1991)004%3c0785:TROACO%3e2.0.CO;2)
- Marcolini G, Koch R, Chimani B, Schöner W, Bellin A, Disse M, Chiogna G (2019) Evaluation of homogenization methods for seasonal snow depth data in the Austrian Alps, 1930–2010. *Int J Climatol* 39:45
- Meehl GA, Senior CA, Eyring V, Flato G, Lamarque J-F, Stouffer RJ, Taylor KE, Schlund M (2020) Context for interpreting equilibrium climate sensitivity and transient climate response from the CMIP6 Earth system models. *Sci Adv* 6:10. <https://doi.org/10.1126/sciadv.aba1981>
- Meseguer-Ruiz O, Ponce-Philimon PI, Quispe-Jofré AS, Guijarro JA, Sarricolea P (2018) Spatial behaviour of daily observed extreme temperatures in Northern Chile (1966–2015): data quality, warming trends, and its orographic and latitudinal effects. *Stoch Environ Res Risk Assess* 32:3503–3523. <https://doi.org/10.1007/s00477-018-1557-6>
- Meusburger K, Steel A, Panagos P, Montanarella L, Alewell C (2012) Spatial and temporal variability of rainfall erosivity factor for Switzerland. *Hydrol Earth Syst Sci* 16:167–177. <https://doi.org/10.5194/hess-16-167-2012>
- Miller JR, Fuller JE, Puma MJ, Finnegan JM (2021) Elevation-dependent warming in the Eastern Siberian Arctic. *Environ Res Lett* 16:024044. <https://doi.org/10.1088/1748-9326/abd5e>
- Muñoz-Sabater J, Dutra E, Agustí-Panareda A, Albergel C, Arduini G, Balsamo G, Boussetta S, Choulga M, Harrigan S, Hersbach H, Martens B, Miralles DG, Piles M, Rodríguez-Fernández NJ, Zsoter E, Buontempo C, Thépaut J-N (2021) ERA5-Land: a state-of-the-art global reanalysis dataset for land applications. *Earth Syst Sci Data Discuss* 1–50. <https://doi.org/10.5194/essd-2021-82>
- New M, Hulme M, Jones P (2000) Representing twentieth-century space–time climate variability Part II Development of 1901–96 Monthly Grids of Terrestrial Surface Climate. *J Clim* 13:2217. [https://doi.org/10.1175/1520-0442\(2000\)013%3c2217:RTCSTC%3e2.0.CO;2](https://doi.org/10.1175/1520-0442(2000)013%3c2217:RTCSTC%3e2.0.CO;2)
- Nimac I, Herceg-Bulić I, Cindrić Kalin K, Perčec Tadić M (2021) Changes in extreme air temperatures in the mid-sized European city situated on southern base of a mountain (Zagreb, Croatia). *Theor Appl Climatol* 13. <https://doi.org/10.1007/s00704-021-03689-8>
- Nimac I, Perčec Tadić M (2017) Complete and homogeneous monthly temperature series for construction of the new 1981–2010 climatological normals for Croatia. *Geofizika* 34:27. <https://doi.org/10.15233/gfz.2017.34.13>
- Odeh IOA, McBratney AB, Chittleborough DJ (1995) Further results on prediction of soil properties from terrain attributes: heterotopic cokriging and regression-kriging. *Geoderma* 67:215–226. [https://doi.org/10.1016/0016-7061\(95\)00007-B](https://doi.org/10.1016/0016-7061(95)00007-B)
- Pandžić K, Likso T (2010) Homogeneity of average annual air temperature time series for Croatia. *Int J Climatol* 30:1215–1225. <https://doi.org/10.1002/joc.1922>
- Pebesma EJ (2004) Multivariable geostatistics in S: the gstat package. *Comput Geosci* 30:683–691
- Pebesma EJ (2014) Gstat user's manual. <http://www.gstat.org/gstat.pdf>. Accessed 2 Feb 2021
- Pepin N, Bradley R, Diaz H, Baraer M, Cáceres B, Forsythe N, Fowler H, Greenwood G, Hashmi M, Liu X, Miller J, Ning L, Ohmura A, Palazzi E, Rangwala I, Schöner W, Severskiy I, Shahgedanova M,

- Wang M, Yang D (2015) Elevation-dependent warming in mountain regions of the world. *Nat Clim Change* 5:424–430. <https://doi.org/10.1038/nclimate2563>
- Perčec Tadić M (2010) Gridded Croatian climatology for 1961–1990. *Theor Appl Climatol* 102:87–103. <https://doi.org/10.1007/s00704-009-0237-3>
- Perry M, Hollis D (2005) The generation of monthly gridded datasets for a range of climatic variables over the UK. *Int J Climatol* 25:1041–1054. <https://doi.org/10.1002/joc.1161>
- Peterson TC, Easterling DR, Karl TR, Groisman P, Nicholls N, Plummer N, Torok S, Auer I, Boehm R, Gullett D, Vincent L, Heino R, Tuomenvirta H, Mestre O, Szentimrey TS, Salinger J, Førland EJ, Hanssen-Bauer I, Alexandersson H, Jones P, Parker D (1998) Homogeneity adjustments of in situ atmospheric climate data: a review. *Int J Climatol* 25
- R Core Team (2020) R: a language and environment for statistical computing. R Foundation for Statistical Computing, Vienna, Austria
- Squintu AA, van der Schrier G, Brugnara Y, Klein Tank A (2019) Homogenization of daily temperature series in the European climate assessment & dataset. *Int J Climatol* 39:1243–1261. <https://doi.org/10.1002/joc.5874>
- Sutton RT, Dong B, Gregory JM (2007) Land/sea warming ratio in response to climate change: IPCC AR4 model results and comparison with observations. *Geophys Res Lett* 34. <https://doi.org/10.1029/2006GL028164>
- Tudoroiu M, Eccel E, Gioli B, Gianelle D, Schume H, Genesio L, Miglietta F (2016) Negative elevation-dependent warming trend in the Eastern Alps. *Environ Res Lett* 11:044021. <https://doi.org/10.1088/1748-9326/11/4/044021>
- van Oldenborgh GJ, Drijfhout S, van Ulden A, Haarsma R, Sterl A, Severijns C, Hazeleger W, Dijkstra H (2009) Western Europe is warming much faster than expected. *Clim Past* 12
- Venema VKC, Mestre O, Aguilar E, Auer I, Guijarro JA, Domonkos P, Vertacnik G, Szentimrey T, Stepanek P, Zahradnicek P, Viarre J, Müller-Westermeier G, Lakatos M, Williams CN, Menne MJ, Lindau R, Rasol D, Rustemeier E, Kolokythas K, Marinova T, Andresen L, Acquaotta F, Fratianni S, Cheval S, Klancar M, Brunetti M, Gruber C, Prohom Duran M, Likso T, Esteban P, Brandsma T (2012) Benchmarking homogenization algorithms for monthly data. *Clim past* 8:89–115. <https://doi.org/10.5194/cp-8-89-2012>
- Verstraeten G, Poesen J, Demarée G, Salles C (2006) Long-term (105 years) variability in rain erosivity as derived from 10-min rainfall depth data for Ukkel (Brussels, Belgium): implications for assessing soil erosion rates *J Geophys Res* 111. <https://doi.org/10.1029/2006JD007169>
- Vicente-Serrano SM, Saz-Sánchez MA, Cuadrat JM (2003) Comparative analysis of interpolation methods in the middle Ebro Valley (Spain): application to annual precipitation and temperature. *Clim Res* 24:161–180. <https://doi.org/10.3354/CR024161>
- Ward JH (1963) Hierarchical grouping to optimize an objective function. *J Am Stat Assoc* 58:236–244. <https://doi.org/10.1080/01621459.1963.10500845>
- Webster R, Oliver MA (2007) *Geostatistics for environmental scientists*, 2nd Edition | Wiley
- Willett K, Williams C, Jolliffe I, Lund R, Alexander L, Brönnimann S, Vincent L, Easterbrook S, Venema V, Berry D, Warren R, Lopardo G, Auchmann R, Aguilar E, Menne M, Gallagher C, Hausfather Z, Thorarindottir T, Thorne P (2014) Concepts for benchmarking of homogenisation algorithm performance on the global scale. *Geosci Instrum Methods Data Syst* 3:1–14. <https://doi.org/10.5194/gi-3-187-2014>
- WMO (2003) Guidelines on climate metadata and homogenization. WMO World Climate and Data Monitoring Programme, Geneva
- WMO (2017a) WMO guidelines on generating a defined set of national climate monitoring products. WMO, Geneva
- WMO (2017b) WMO guidelines on the calculation of climate Normals. WMO, Geneva
- WMO (2020) Guidelines on homogenization. WMO Task Team on Homogenization of the Commission for Climatology, Geneva
- Zaninović K, Gajić-Čapka M, Perčec Tadić M, Vučetić M, Milković J, Bajjić A, Cindrić K, Cvitan L, Katušin Z, Kaučić D, Likso T, Lončar E, Lončar Ž, Mihajlović D, Pandžić K, Patarčić M, Srnc L, Vučetić V (2008) Klimatski atlas Hrvatske / Climate atlas of Croatia 1961–1990, 1971–2000. Državni hidrometeorološki zavod. http://klima.hr/razno/publikacije/klimatski_atlas_hrvatske.pdf

Publisher's note Springer Nature remains neutral with regard to jurisdictional claims in published maps and institutional affiliations.